Investigating the CCAAT/Enhancer-Binding Protein Beta-Regulated Tumour-Derived Secretome in Cancer Cachexia

Ayesha Syed

Thesis submitted to the University of Ottawa
in partial Fulfillment of the requirements for the
Master's degree in Cellular and Molecular Medicine

Department of Cellular and Molecular Medicine
Faculty of Medicine
University of Ottawa

ACKNOWLEDGEMENTS

First and foremost, I would like to thank my parents, Tariq Syed and Rukshanda Ahmad, for their constant encouragement, love, and support throughout my life. Their sacrifices, strength, and unwavering belief in me have been the foundation of every success I have had. I am also incredibly grateful to all my family members, including my brothers Hamza and Mustafa, my sisters Reem, Danya and Sarah, and my dear uncle and aunt, Sultan and Monazza, for their encouragement, prayers, and support during this journey.

I would like to extend my sincere gratitude to Dr. Nadine Wiper-Bergeron for her continuous support, mentorship, and guidance throughout my graduate studies. From my early days in the TMM program to the completion of this thesis, your feedback and direction have helped shape my development as a scientist. Thank you for your time, patience, and for always encouraging me to think critically and approach problems with curiosity. I am especially grateful for the opportunities you provided me within the lab and the trust you placed in me to take on independent work. Your mentorship has had a meaningful impact on both my academic and professional growth.

I would like to thank my thesis advisory committee members, Dr. Dylan Burger and Dr. Celine Aguer, for their thoughtful feedback, consistent support, and valuable insights throughout the course of this project. Your guidance during committee meetings helped strengthen both the scientific direction and the clarity of my research. Thank you for your encouragement and for contributing to an environment that supported both my academic development and scientific curiosity.

To Aisha Saleh, my mentor, role model, and dear friend, thank you for your unwavering support, guidance, and encouragement throughout this journey. Whether it was troubleshooting

experiments, powering through late night lab sessions, enjoying lunch together, or offering advice, your presence made all the difference. I have learned so much from the way you approach research, resilience, and life. I am endlessly proud of everything you have accomplished, and I can't wait to call you Dr. Saleh soon.

To all my lab members, thank you for your support, collaboration, and for making the lab a positive and welcoming environment. I am grateful for your help, advice, and the many shared moments that made this experience more meaningful. I am also thankful for the laughs and sense of community you created, which made the lab feel like home.

I would like to thank Andrew Macklin from the OHRI Proteomics Core Facility for his assistance with mass spectrometry and for his consistent support throughout the proteomics portion of this project. I am also grateful to the Burger Lab for their technical expertise and guidance during the extracellular vesicle analyses.

Finally, I gratefully acknowledge the financial support provided by the Ontario Graduate Scholarship and the Queen Elizabeth II Graduate Scholarship in Science and Technology, which enabled me to carry out this research. Also, to all my dear friends, and to my beloved cats Nalah and Ayubi, thank you for keeping me grounded and bringing joy during these moments.

In closing, I am sincerely grateful to everyone who contributed to this work, whether through mentorship, guidance, or personal support. This thesis reflects not only my efforts but also the generosity, expertise, and encouragement of many individuals along the way.

TABLE OF CONTENTS

ACKNOWLEDGEMENTS ii

ABSTRACT vi

LEGEND vii

LIST OF FIGURES xii

LIST OF TABLES xiii

1. INTRODUCTION 1

1.1 Cancer cachexia overview 1

1.2 The dual "Janus" role of CCAAT/enhancer-binding protein β C/EBPβ in cancer 2

1.3 Role of CCAAT/enhancer-binding protein β (C/EBPβ) in cancer cachexia 3

1.4 Secretome components and secretion pathways 4

1.5 Extracellular vesicles 4

1.6 EVs in the context of cancer cachexia 5

1.7 Analysis of the tumour secretome via enzymatic biotinylation 5

1.8 Current secretome analysis challenges 6

2. OBJECTIVES AND HYPOTHESIS 8

2.1 Hypothesis of Project 8

2.2 Aims of Project 8

2.3 Overall Objective of Project 9

3. METHODS 10

3.1 Cell Culture and Conditioned Medium Experiments 10

3.2 Immunofluorescence and Myotube Measurements 10

3.3 Western Blot Preparation 11

3.4 Isolation of Extracellular Vesicles and Nanoparticle Tracking Analysis 11

3.5 Mammalian Cell culture, Transfection, and Stable Cell Line Generation 12

3.6 Sample Preparation for Proteomics 13

3.7 Data Quantification and Analysis 13

4. RESEARCH RESULTS 15

4.1 Aim 1: Characterize the atrophic potential of conditioned media and secretome fractions from multiple cancer cell lines, and assess the relationship between atrophy induction and C/EBPβ expression 15

4.1.1 Establishing atrophic models and their relationship to C/EBPβ expression in vitro: 15
4.1.2 Concentration and sizes of EVs in atrophic and non-atrophic in vitro models 17
4.1.3 LLC derived EVs and apoptotic bodies contribute to atrophy in vitro 19
4.1.4 EVs derived from MC38 and EL4 do not cause atrophy in vitro 22
4.2 Aim 2: Develop a TurboID-based system to label and identify secreted proteins in a cachexia-inducing cancer model, and link identified proteins to C/EBPβ-dependent gene expression changes. 24
4.2.1 Validation of successful intracellular integration of TurboID in 7 murine cancer cell line constructs 25
4.2.2 Validation of secretion of biotin-tagged proteins and streptavidin-enrichment capture 29
4.2.3 LLC WT with integrated TurboID vector derived CM causes atrophy in vitro 32
4.2.4 Mass spectrometry data reveals the capture of novel secreted proteins 34
4.2.5. Secreted proteins linked to secretory pathways and distinct secretome between LLC WT and MC38 WT secretome. 43
4.2.6. Secreted proteins downregulated and upregulated in C/EBPβ OE/KO RNA sequencing data 45
5. DISCUSSION OF RESULTS 48
5.1 Summary of Key Findings 48
5.1.1 C/EBPβ expression correlates with atrophy in a cell specific manner 49
5.1.2 Atrophy-inducing and non-atrophic cancer cell lines release similar concentrations of EVs but differ in their EV size distributions 52
5.1.3 LLC derived extracellular vesicles, and apoptotic bodies contribute to wasting in vitro 53
5.1.4 EVs derived from non-atrophic cell lines do not contribute to wasting in vitro 54
5.1.5 TurboID machinery successfully labels intracellular proteins and biotin tags allow for the successful capture of secreted proteins 55
5.1.6 LLC WT secretome reveals capture of 24 proteins 56
5.1.7 Knockout of C/EBPβ is critical in modulating the LLC secretome 58
5.1.8 Future use of TurboID for in vivo proteomic mapping and understanding of communication networks 59
6. CONCLUSION 61
7. BIBLIOGRAPHY 63

ABSTRACT

Cancer cachexia is a paraneoplastic syndrome characterized by muscle wasting, often driven by cachexia-inducing factors (CIFs)[1,2]. This thesis investigates the role of CCAAT/enhancer-binding protein β (C/EBPβ) in regulating the cancer secretome responsible for inducing cachexia[3]. Using murine cancer cell lines, the study assessed the atrophic potential of conditioned media, extracellular vesicles (EVs), and apoptotic bodies, linking their effects to C/EBPβ expression. A TurboID-based enzymatic biotinylation system was developed to tag and isolate secreted proteins for proteomic profiling[4].

Mass spectrometry revealed 24 unique secreted proteins, many associated with vesicular transport, whose expression was modulated by C/EBPβ. RNA-sequencing analysis confirmed that C/EBPβ knockout altered secretome composition more significantly than overexpression. These findings support C/EBPβ as a key regulator of cachexia-inducing factors and validate TurboID as a powerful tool for *in vitro* secretome profiling. This work advances our understanding of tumor-host communication in cachexia and identifies potential targets for therapeutic intervention.

LEGEND

AF188	Alexa Fluor 488
ANOVA	Analysis Of Variance
ARHGAP1	Rho Gtpase-Activating Protein 1
ASNS	Asparagine Synthetase
ATCC	American Type Culture Collection
ATL3	Atlastin-3
BCAP31	B-Cell Receptor-Associated Protein 31
BCL2L13	Bcl-2-Like Protein 13
B16	Melanoma
C/EBPs	CCAAT/Enhancer-Binding Proteins
C/EBPβ	CCAAT/Enhancer-Binding Protein Beta
CAST	Calpastatin
CD81	Cluster Of Differentiation 81
CD9	Cluster Of Differentiation 9
CIF	Cachexia Inducing Factor
CM	Conditioned Medium
CRISPR	Clustered Regularly Interspaced Short Palindromic Repeats
CRISPR-Cas9	CRISPR-Associated Protein 9
CT2A	Murine Glioma Cell Line
CYPB	Cyclophilin B
C2C12	Myoblast cell line
DAPI	4',6-Diamidino-2-Phenylindole

DM	Differentiation Medium
DMEM	Dulbecco's Modified Eagle Medium
DNA	Deoxyribonucleic Acid
DSHB	Developmental Studies Hybridoma Bank
D4	Day 4
D6	Day 6
EGFR	Epidermal Growth Factor Receptor
EL4	Murine T Cell Lymphoma Cell Line
EMD	Emerin
ER	Endoplasmic Reticulum
EV	Extracellular Vesicle
FBS	Fetal Bovine Serum
FDR	False Discovery Rate
GL261	Murine Glioma Cell Line
GM	Growth Medium
GO	Gene Ontology
GOF	Gain Of Function
HEK	Human Embryonic Kidney Cells
HRP	Horseradish Peroxidase
HYOU1	Hypoxia Upregulated 1
ID8	Ovarian Surface Epithelial Cell Line
IFN-γ	Interferon Gamma
IGBP1	Immunoglobulin-Binding Protein 1

IL-1β	Interleukin-1 beta
IL-4	Interleukin-4
IL-6	Interleukin-6
JPT2	Jupiter Microtubule Associated Homolog 2
KO	Knockout
LAP	Liver-Enriched Activator Protein
LBR	Delta(14)-Sterol Reductase Lbr
LIP	Liver-Enriched Inhibitory Protein
LLC	Lewis Lunch Carcinoma
LOF	Loss Of Function
MAP4	Microtubule-Associated Protein 4
MAPK	Mitogen-Activated Protein Kinases
MC38	Colon Adenocarcinoma Cells
MF20	Myosin Heavy Chain Antibody
MS	Mass Spectrometry
MV	Microvesicle
MYHC	Myosin Heavy Chain
MYOF	Myoferlin
NTA	Nanoparticle Tracking Analysis
OE	Overexpression
OHRI	Ottawa Hospital Research Institute
O/N	Overnight
PAK2	Serine/Threonine-Protein Kinase PAK 2

PBS	Phosphate Buffered Saline
PC1	First Principal Component
PC2	Second Principal Component
PCA	Principal Component Analysis Plot
PDCD6IP	Programmed Cell Death 6-Interacting Protein
PEI	Polyethylenimine
PI	Phosphoinositide
PI3K/AKT	Phosphatidylinositol 3-Kinase/Protein Kinase B
RNA	Ribonucleic Acid
RTK/RAS	Receptor Tyrosine Kinase/Ras
SEC22B	Vesicle-Trafficking Protein SEC22b
SEC23A	Protein Transport Protein Sec23A
SEM	Standard Error Of The Mean
SET	Protein SET
SLC16A1	Monocarboxylate Transporter 1
SMSC	Skeletal Muscle Satellite Cells
SRPRA	Signal Recognition Particle Receptor Subunit Alpha
ST101	Lucicebtide
STRING	Search Tool For The Retrieval Of Interacting Genes/Proteins
TF	Transcription Factor
TFRC	Transferrin Receptor Protein 1
TGF-β	Transforming Growth Factor-Beta
TME	Tumour Microenvironment

TMPO	Lamina-Associated Polypeptide 2
TNF-α	Tumour Necrosis Factor Alpha
TXN	Thioredoxin
UC	Unconditioned
UPP	Ubiquitin-Proteasome Pathway
UPR	Unfolded Protein Response
VAPA	Vesicle-Associated Membrane Protein-Associated Protein A
WT	Wild Type

LIST OF FIGURES

Figure 1. Cancer conditioned medium (CM) experiment and expression of C/EBPβ results *in vitro.*

Figure 2. Average concentration and median size of EVs.

Figure 3. LLC derived EVs are critical for myotube atrophy *in vitro.*

Figure 4. LLC derived apoptotic bodies contribute to atrophy *in vitro*

Figure 5. MC38 derived EVs do not contribute to atrophy *in vitro.*

Figure 6. EL4 derived EVs do not contribute to atrophy *in vitro.*

Figure 7. Validation of TurboID vector transfection into seven murine cancer cell line constructs.

Figure 8. Validation of secreted biotin enriched protein capture.

Figure 9. Cancer conditioned medium (CM) experiment of LLC WT with TurboID vector

Figure 10. Mass spectrometry results of LLC WT secreted proteins.

Figure 11. Characterization of LLC WT secreted proteins.

Figure 12. LLC WT secreted proteins gene ontology biological processes and cellular compartmentalization, and heatmap of RNA expression of secreted proteins in LLC WT and MC38 WT cells.

Figure 13. Heatmap of RNA expression of secreted proteins in LLC C/EBPβ Overexpression (OE) and Knockout (KO).

LIST OF TABLES

Table 1. Summary of the 24 proteins identified from all 3 trials.

1. INTRODUCTION

1.1 Cancer cachexia overview

Cancer is a heterogeneous disease characterized by uncontrolled growth of cells that evade the host's immune system,[5] and go on to invade and interfere with normal tissue and organ function[6]. In Canada, two out of five individuals will be diagnosed with cancer in their lifetime[7], with an estimated 239,100 new cancer cases in 2023[8]. Cancer not only impacts normal organ function, but also often leads to a paraneoplastic syndrome (i.e. a secondary disease brought on by the cancer) known as cancer cachexia[2]. Cancer cachexia affects over 80% of cancer patients, with a direct mortality rate between 22% to 30%[9,10]. Cachexia is frequent in advanced pancreatic[11], lung[12], gastrointestinal[12], colorectal[13], and head[13] and neck cancers[13], where it is associated with poor response to chemotherapy and reduced survival[1]. Clinically, this wasting syndrome is diagnosed by decreased muscle mass, weight loss, growth disorders in children, and loss of appetite[14].

The development of cachexia involves a multitude of mechanisms including altered host metabolic responses, anorexia, and decreased secretion of host anabolic hormones[1]. Many of such development is attributed to the complex interactions between the host and the tumour cells, where tumour-derived factors, also known as cachexia-inducing factors (CIFs), such as cytokines, hormones, and growth factors directly or indirectly affect appetite regulation, metabolism, and protein synthesis[15]. These interactions between the host and tumour cells, leads to systemic inflammation thought to arise from tumour production of proinflammatory and procachectic factors[16]. Although, researchers have identified a variety of potential CIFs[15], a common cachexia-inducing secretome has not been identified due to the differences in tumour types, secreted CIFs, and prevalence of cachexia[17].

In addition, the host, in response to the tumour, may itself produce a variety of pro-inflammatory cytokines which may drive cachexia[16], including TNF-α, IL-6, IFN-γ, and IL-1β which are increased in cachexia and have been demonstrated to be key players in the pathogenesis of the disease[3,16,18]. However, despite a described role of these cytokines in inducing muscle wasting via proteolysis and lipolysis, anti-cytokine therapies have not been effective in all cancer patients with a lack of overall positive outcomes[19,20]. The inhibition of many anti-cytokine therapies does not stop or reverse the progression of cancer cachexia[1]. For this reason, current therapies focus on palliative care with aims of reducing distress for families and patients[1].

1.2 The dual "Janus" role of CCAAT/enhancer-binding protein β C/EBPβ in cancer

Constitutive expression and/or activation of transcription factors (TFs) is required for growth and survival of cancers as cancer is a multi-step process[21]. Poor prognosis and chemoresistance is associated with high expression of some TFs[21]. Researchers are looking into targetting TFs as a better strategy to treat cancer[21,22]. Recently, the CCAAT/enhancer-binding protein β (C/EBPβ)[3], was identified as a hierarchical TF responsible for the cachexia-inducing secretome[3].

C/EBPβ is part of a family of six structurally homologous transcription factors known as CCAAT-enhancer-binding proteins (C/EBPs)[23]. C/EBPs can act as both tumour suppressors and promotors[23], a phenomenon referred to as "*Janus*" which is named after the Roman god Janus, depicted with two opposing faces[24]. This duality is influenced by several factors including isoform expression in cell types, presence of inhibitory elements, dimerization patterns (homo- or heterodimerization), and their capacity to supress the expression of other tumour suppressors[23]. In general, C/EBPβ is involved in regulating various cellular processes such as

proliferation, differentiation, apoptosis, and immunity[25] in healthy tissues and interestingly most cancers express C/EBPβ[26–28].

C/EBPβ regulates genes important for immune and inflammatory responses (i.e. IL-6, IL-4, IL-5, TNF-α), macrophage and B-cell differentiation, nervous system function, and activation of genes that confer multidrug resistance[23]. It plays a dual "*Janus*" role via its anti-oncogenic and pro-oncogenic effects[23]. The presences of different isoforms of C/EBPβ can determine its pro- and anti-tumorigenic activities[23]. C/EBPβ exists as 3 isoforms: C/EBPβ p38 or Liver Activating Protein* (LAP*), C/EBPβ p33 or Liver Activating Protein (LAP), and C/EBPβ p20 or Liver Inhibiting Protein (LIP)[23]. In general, LAP and LIP promote cell proliferation and tumour progression, whereas LAP* is involved in terminal proliferation[23]. For normal cell development and growth, proper ratios of these 3 isoforms are necessary[23].

1.3 Role of CCAAT/enhancer-binding protein β (C/EBPβ) in cancer cachexia

Previous research carried out by the Wiper-Bergeron lab demonstrated that C/EBPβ is a central regulator of cancer cachexia by driving the expression of atrophy-inducing factors secreted by tumours[3]. The overexpression of C/EBPβ in myoblasts resulted in the production of a secretome that inhibited myotube maturation and myogenic differentiation leading to the identification of 260 secreted protein genes that are up regulated[3].

To assess the potential role of C/EBPβ in the expression of CIFs, loss of function and gain of function models of C/EBPβ were established in the cachectic Lewis lung carcinoma (LLC), and non-cachectic T-cell lymphoblastoma (EL4) tumour lines[3]. LLC have high expression of C/EBPβ, whereas EL4s have low/negligible expression of C/EBPβ[3]. Loss of C/EBPβ in LLCs resulted in a less cachectic phenotype when its conditioned medium was placed

on myotubes in culture, suggesting that CIFs secreted by LLC require C/EBPβ[3]. Similarly, overexpression of C/EBPβ in EL4 converted a non-cachectic secretome into one that promotes wasting as observed by an inhibition of differentiation and reduced myotube diameter *in vitro*, and muscle wasting *in vivo*[3]. These results provide an initial understanding of C/EBPβ's role in producing the cachexia-inducing secretome[3], yet the complexity of the secretome remains largely unexplored, and selecting specific tumor types or different methodological approaches may lead to more comprehensive understanding of its biological function[17].

1.4 Secretome components and secretion pathways

In cancer, the abnormal secretion of molecules is known as the cancer cell secretome which contributes significantly to tumour development, progression, and eventual metastasis[29]. Every stage of the tumorigenic cascade is influenced by the cancer cell secretome[29]. The secretome consists of cytokines, chemokines, coagulation factors, hormones, growth factors, microRNA, glycoproteins, and enzymes which can be secreted individually or secreted via vesicles such as extracellular vesicles[29]. There are two pathways generally used in secretion[29]. The first is the "classical" secretory pathway where secretory vesicles are packaged with molecules that then fuse with the plasma membrane to expel their contents into the microenvironment[29]. Other "non-classical" pathways have also been observed where proteins are directly secreted from the Endoplasmic Reticulum (ER)[29].

1.5 Extracellular vesicles

Cells secrete lipid bound vesicles known as extracellular vesicles (EVs) into the surrounding extracellular environments[30]. Originally EVs were thought to be the method of elimination of

proteins, lipids, and RNA from cells[31]. Now, the role of EVs is described as a means of intercellular communication[31].

There are three main subtypes of EVs from largest to smallest in size: apoptotic bodies (50 – 5000 nm), microvesicles (MVs) (100 nm – 1 μm), and exosomes (30 – 150 nm)[30]. Dying cells will release apoptotic bodies which contain chromatin, intact organelles, and glycosylated proteins[30]. MVs are formed by the pinching of the plasma membrane via outward budding, and often carry cytosolic, plasma membrane-associated, post translational modification proteins[30]. Exosomes are formed via the endosomal route and often contain glycoproteins[30]. There are also a variety of methods to isolate EVs including ultracentrifugation which is considered to be the gold standard, density gradient techniques, and precipitation kits[30].

1.6 EVs in the context of cancer cachexia

EVs have been implicated in cancer via their various roles in cell-cell communication, tissue repair, epigenetic regulation, and immune response[32]. Where tumour derived EVs can influence the function of remote tissues (i.e skeletal muscle and adipose tissue) and organs by acting as a means of communication between cancer and such cell types[33]. Recent research has revealed that cancer-derived EVs can induce cachexia by promoting muscle atrophy via increases in muscle apoptosis and proteolysis, and decreases in myogenesis, once these EVs are taken up by muscle cells[33–35]. However, the EV packaged secretome has not been characterized for tumour types in the context of cancer cachexia, and more knowledge is needed on the content and function of EVs themselves in cancer cachexia[33].

1.7 Analysis of the tumour secretome via enzymatic biotinylation

Current methodologies used to investigate the cachexia-inducing tumour secretome involve the use of label-free proteomics[36,37], a technique that allows for analysis of biological

samples over a larger scale[38]. This technique is commonly used to determine biomarkers[37] and conduct large-scale proteome profiling[36]. However, quantification of label-free proteomic results in higher amounts of variances than labeled proteomics[39–41], another technique that allows for more accurate quantification[41]. Labeled proteomics, such as biotinylation-based proteomics, increases secretome characterization via mass spectrometry (MS) *in vitro*, as secreted factors are more easily identifiable[42], and offers more insight into the secretome by mapping proteins *in vivo*[43,44]. This technique involves the use of enzymatic biotin ligases that when introduced into the endoplasmic reticulum (ER) allow for the tagging of proteins as they are produced[45]. Conversely, this technique could potentially allow for the mapping of extracellular vesicles (EVs), which are important mediators of intercellular communication via their trafficking of protein cargo[46], especially considering the emerging role of EVs in driving cancer cachexia[32,33].

1.8 Current secretome analysis challenges

Furthermore, one of the largest challenges associated with *in vitro* secretome analysis is sample preparation[47]. Often the media collected from cancer cells is contaminated with serum-based proteins which affects the purity of the samples sent for MS[48]. To avoid the contamination from serum, serum depletion techniques are utilized[49] though serum deprivation has been documented to interfere with results as some serum constituents remain even after depletion and rinses and serum-free cultures can directly impact cell behaviour and as such their secretomes[48]. Additionally, discrimination between secreted proteins and non-secreted proteins remains a significant unresolved issue when it comes to *in vitro* secretome analysis[48]. For this reason, biotinylated-based proteomics serves as a potential technique to investigate the cancer-cachexia secretome via selective isolation of proteins and EVs in complete culture medium that are produced by cancer cell lines *in vitro*[48], and potential secretome mapping *in vivo*[43,44].

By using the stated techniques, more insight on the factors regulated by C/EBPβ will be revealed, as currently regulation of such factors is unknown, despite results published by the Wiper-Bergeron lab that have established models of cachectic (i.e LLC) and non-cachectic (i.e EL4) cancers via myotube atrophy analysis and expression of C/EBPβ[3]. Thus, by using the stated techniques, a core C/EBPβ-regulated gene signature can be determined in the future via a comparative secretome analysis of multiple cachexia-inducing and non-cachectic tumours using MS.

2. OBJECTIVES AND HYPOTHESIS

2.1 Hypothesis of Project

The overarching hypothesis of this MSc. thesis is that ***cancer cell lines with elevated C/EBPβ expression promote cachectic phenotypes*** *through the secretion of* ***specific proteins and vesicular components that target muscle.***

2.2 Aims of Project

The following research aims will be used to test the hypothesis:

1. Characterize the atrophic potential of conditioned media and secretome fractions from multiple cancer cell lines and assess the relationship between atrophy induction and C/EBPβ expression. We predict that:
    1. Cancer cell lines with higher C/EBPβ expression will induce greater myotube atrophy compared to lines with lower C/EBPβ expression[3].
    2. Cachexia-inducing cancer cell lines will exhibit higher concentrations of extracellular vesicles and/or shifts in vesicle size distribution relative to non-cachectic lines.
2. Develop a TurboID-based system to label and identify secreted proteins in a cachexia-inducing cancer model, and link identified proteins to C/EBPβ-dependent gene expression changes. We predict that:
    1. TurboID-based labeling will successfully identify secreted proteins specifically enriched in cachexia-inducing cancer cells and several identified secreted proteins will show C/EBPβ-dependent expression changes.

2.3 Overall Objective of Project

Thus, the overall objective is to examine components of the **cancer cell secretome** and **develop a biotin-based method to profile** the secretome of cachexia-inducing cancers, with a focus on **linking secreted factors to C/EBPβ expression and regulation**.

3. METHODS

3.1 Cell Culture and Conditioned Medium Experiments

C2C12 myoblasts (ATCC) were seeded in DMEM (Wisent) supplemented with 10% FBS (Wisent) growth media (GM). To induce differentiation 48 hours post seeding, differentiation media (DM: DMEM supplemented with 10% horse serum (Sigma)) replaced the GM and myotubes were left to form for 4 days (D4). Alongside, the following cancer cell lines (ATCC) were seeded to grow to ~80% confluence in 48 hours: Lewis lung carcinoma (LLC), murine T cell lymphoma (EL4), colorectal carcinoma (MC38), glioma (GL261), glioblastoma (CT2A), melanoma (B16), and ovarian surface epithelial cell line (ID8).

Subsequently, conditioned media (CM) was collected after 48 hours, and cancer cells were collected to assess C/EBPβ protein level. C2C12 myotubes were treated at ratio of 1:1 cancer CM: GM and control received only GM. For extracellular vesicle (EV) conditioned medium experiments, the same protocol was used as above with two added treatments, direct treatment with EV's and EV-free CM in a 1:1 condition:GM ratio. Additionally, CM was concentrated via Amicon® Ultra Centrifugal Filter, 3 kDa MWCO (UFC900324, Millipore Sigma) for 1 hour according to manufacture recommendations and then re-suspended in fresh GM. After 48 hours, C2C12 myotubes were fixed for immunofluorescence on day 6 (D6).

3.2 Immunofluorescence and Myotube Measurements

Cells were fixed in cold methanol (-20°C). Myotubes were incubated with primary antibody against myosin heavy chain (MyHC) (MF20, DSHB, 1:50) overnight (ON) at 4°C on shaker. Secondary antibody Cy3 anti-mouse (anti-mouse Cy3, Jackson ImmunoResearch, 1:500) was used at room temperature. Cancer cell lines transfected with TurboID were incubated with

AF488 Streptavidin antibody (Alexa fluro 488 Streptavidin, Invitrogen, 1:50) at room temperature. Counterstaining for nuclei was done with DAPI. AxioObserver 7 microscope (Zeiss) was used with the 10x objective to capture 5 random images. For myotube size, myotube diameter (μM) was measured from 5 random images as an average of three measurements (at the two ends and centre of the myotubes) via Fiji (ImageJ) software and then presented as averages. Average percent (%) of MyHC positive area was calculated via Fiji for each condition.

3.3 Western Blot Preparation

Whole cell extracts were prepared using a whole cell extract buffer for the following: C2C12, MC38, EL4, LLC, GL261, ID8, CT2A, B16 cell lines. The following antibodies were used for detection C/EBPβ (Abcam, ab32358, 1:500), Cyclophilin B (Abcam, ab16045, 1:5000)[3], or Streptavidin (Invitrogen, S911, 0.3 μg/mL), V5 Tag Monoclonal Antibody (Invitrogen, SV5-Pk1, 1:500), Calnexin (Invitrogen, MA3-027, 1:500), CD9 (Thermo Fisher, 14-0091-82, 1:500), and CD81 (Thermo Fisher, MA5-32333, 1:1000). Chemiluminescence was detected with the ChemiDocTM system (Bio-Rad). Image Lab software (Bio-Rad) was used for protein quantification and blot cropping[3].

3.4 Isolation of Extracellular Vesicles and Nanoparticle Tracking Analysis

Cancer cell lines were seeded at 80-90% confluence in GM for 24 hours, then placed in EV-depleted media (Thermo Fisher Scientific) for 24 hours, followed by centrifugation and ultracentrifugation steps. Isolated EVs were resuspended in ice cold 1X PBS[50]. Analysis was conducted as described by Dylan Burger lab[50], with the following differences: dilutions of EV isolates (ranging from 1:1000 to 1:8000 dilutions) were analyzed with Zetaview software (version 8.03.08) by ZetaView PMX 110 Multiple Parameter Particle Tracking Analyzer (Particle Metrix, Meerbusch, Germany).

Protein extraction of EVs were conducted according to Dylan Burger Lab protocols[50]. EV presence was confirmed via NTA and western blots using the following antibodies CD9, CD81, and Calnexin. Chemiluminescence was detected with the ChemiDocTM system (Bio-Rad). Image Lab software (Bio-Rad) was used for protein quantification and blot cropping.

3.5 Mammalian Cell culture, Transfection, and Stable Cell Line Generation

Plasmids used for transfection were C1(1-29)-TurboID-V5_pLX304 plasmid, a gift from Alice Ting (Addgene plasmid #107175), psPAX2 plasmid (Addgene plasmid # 12260) and pMD2.G (Addgene plasmid # 12259) were gifts from Didier Trono. Plasmids were grown according to their respective manufacturer's instructions, and DNA was isolated via PureLink™ HiPure Plasmid Maxiprep Kit (ThermoFisher Scientific)[51]. Absorbances were collected via NanoDrop 2000 Spectrophotometer (ThermoFisher Scientific).

LOF/GOF models were generated by A. Saleh. To generate LOF/GOF models, CRISPR-Cas9 was used to knockout C/EBPβ[52], and retroviral infections, where cDNA encoding full-length C/EBPβ were cloned into the pLXSN vector (Clontech) to generate overexpression of C/EBPβ as described in established protocols[3,53].

To generate lentivirus, HEK 293T (ATCC) cells were seeded at 80-100% confluence in GM (DMEM, 10% FBS, 1% penicillin/streptomycin)[51]. Transfection was conducted with 7.5ug of C1(1-29)-TurboID-V5_pLX304, 2.5ug of psPAX2, and 0.75ug of pDM2.G with polyethylenimine (PEI) in serum-free media for 5 hours and then replaced with GM[4]. Lentivirus was collected for 4 days, followed by filtration (0.45-μm filter) and virus precipitation (Virus precipitation kit, Benchmark Bioscience)[4]. Cancer cell lines were infected at ~60% to 90% followed with 10 days of selection with blasticidin in GM[4].

3.6 Sample Preparation for Proteomics

Transfected cell lines were supplemented with 50 μM of biotin for 48 hours, followed by 1x PBS washes, and then new GM for 48 hours. CM was concentrated via Amicon® Ultra Centrifugal Filter, 3 kDa MWCO (UFC900324, Millipore Sigma) for 1 hour according to manufacture recommendations. Remaining lysates were incubated with Pierce™ Streptavidin Magnetic Beads (Thermo Fisher Scientific) following manufacture's protocols at 4°C O/N on shaker. Western blots confirmed the presences of biotinylated proteins via Streptavidin-HRP. For negative controls, addition of exogenous biotin was omitted.

Biotinylated factors were kept on streptavidin magnetic beads for on-bead trypsinization in 50mM Ammonium Bicarbonate (pH = 7) and sent for mass spectrometry (MS) to the Ottawa Hospital Research Institute (OHRI) proteomics facility according to the facility's sample preparation requirements[54]. MS quantification was conducted with a FDR cut-off of 1% and minimum peptide threshold of 2.

Proteins that were found in control samples were considered background proteins and removed if found in list of experimental condition proteins for trial 1, 2, and 3. Any protein identified as contaminant proteins were also removed if found in experimental condition proteins. This was done to generate a list (n=3) of proteins captured specifically from the cell line secretome of interest. Protein list was compared to A. Saleh RNA sequencing (unpublished data) of C/EBPβ GOF/LOF secreted factors and control secreted factors.

3.7 Data Quantification and Analysis

Data are presented as the mean ± SEM (standard error of the mean)[3,55]. A one-way ANOVA was performed where applicable, followed by post hoc multiple comparison tests (Tukey's or

Dunnett's, as indicated) to determine group-wise significance. Unpaired two-tailed t-tests were used for direct two-group comparisons. Statistical analyses were conducted using GraphPad Prism. Significance was defined at a cut-off of $p < 0.05$[55]. Where appropriate, compact letter were displayed or asterisks (*$p < 0.05$, **$p < 0.01$, ***$p < 0.001$, ****$p < 0.0001$). The investigator was not blinded to experimental conditions.

4. RESEARCH RESULTS

4.1 Aim 1: Characterize the atrophic potential of conditioned media and secretome fractions from multiple cancer cell lines, and assess the relationship between atrophy induction and C/EBPβ expression

4.1.1 Establishing atrophic models and their relationship to C/EBPβ expression in vitro:

The first step in the objective of determining a C/EBPβ-regulated gene signature requires an understanding of which cancer cell lines are considered to be atrophic and non-atrophic. For this reason, the established protocol by the Wiper-Bergeron Lab (Figure 1. A) was used to identify models of atrophic and non-atrophic cancer cell lines with respect to C/EBPβ protein expression[3].

The 7 murine tumour cell lines (LLC, MC38, B16, GL261, CT2A, ID8, and EL4) were organized in accordance with their ability to induce atrophy (i.e as observed via decreases in myotube diameter compared to Day 4 (D4) and Day 6 (D6) controls (Figure 1. B - D) and their respective levels of C/EBPβ expression (Figure 1, E – F)). As shown previously, myotubes incubated with conditioned media (CM) from LLC cells results in a significant decrease in myotube diameter relative to D6 controls (Fig 1. C)[3]. Similarly, incubation with EL4 derived CM reduces myotube diameter but not significantly like LLC derived CM (Fig. 1. B, C)[3].

C/EBPβ expression levels range from highest to lowest: MC38, LLC, GL261, B16, CT2A, ID8, and EL4 (Figure 1. E, F). Despite its high C/EBPβ expression level, MC38 was not found to be the most atrophic in culture, however it does produce significant cachexia *in vivo* (N. Strong, unpublished). The difference in cachexia induction may be due to MC38 relying on a distinct cell population to drive cachexia indirectly, whereas LLC directly targets C2C12 cells to cause muscle wasting.

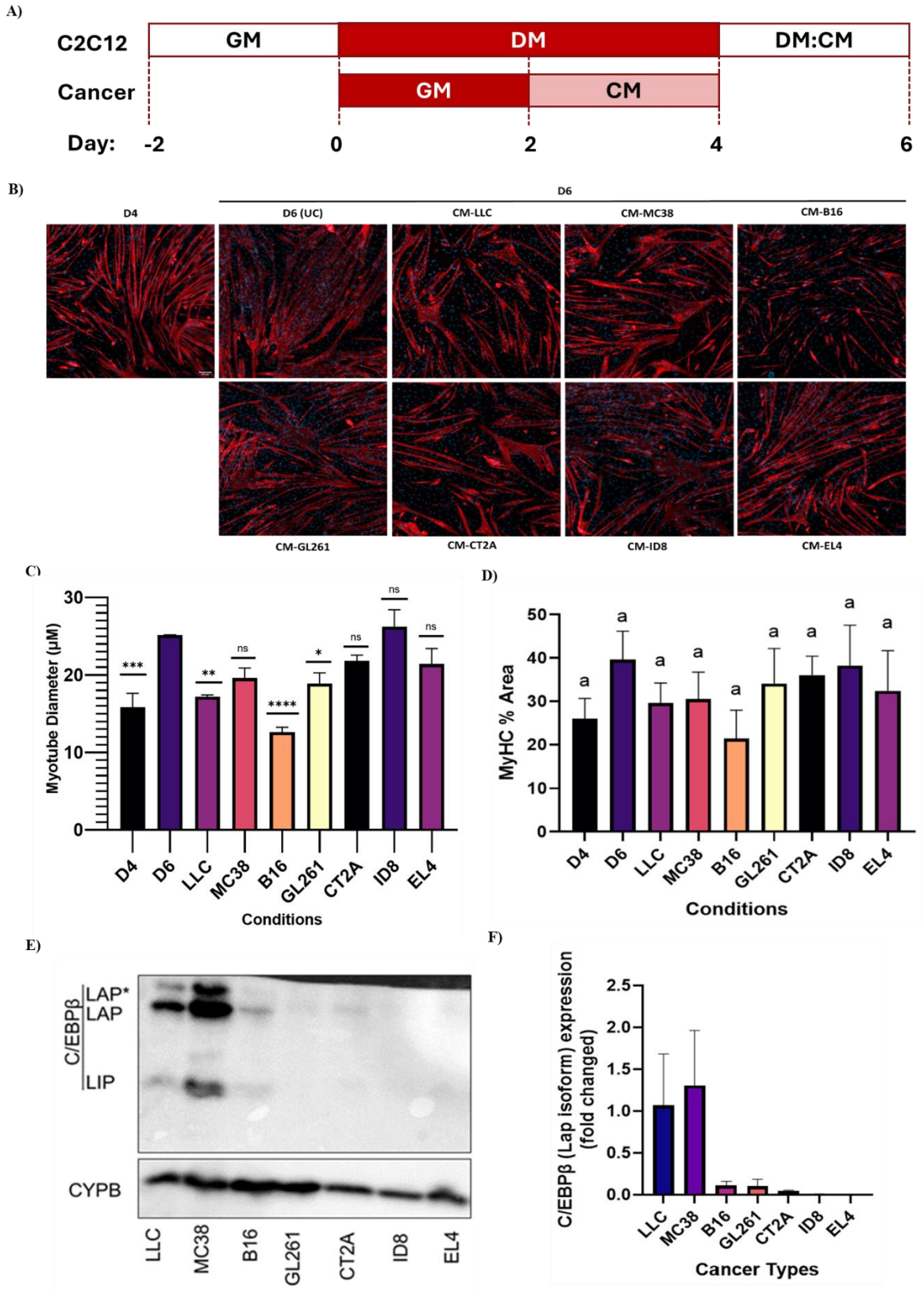

Figure 1. Cancer conditioned medium (CM) experiment and expression of C/EBPβ results *in vitro*. A) Schematic representation of the experimental workflow. C2C12 myoblasts were

cultured to confluency in growth media (GM) and subsequently differentiated in low-serum differentiation media (DM) for 4 days (D4). In parallel, cancer cells were grown to confluency in GM for 2 days, after which the media was replaced to collect conditioned media (CM). On Day 4 (D4), differentiated myotubes were treated for an additional two days (until Day 6, D6) with a 1:1 mixture of conditioned media (CM) and fresh differentiation media (DM) for experimental conditions, or a 1:1 mixture of DM and growth media (GM) for controls. B) Immunofluorescence images of day 6 (D6) myotubes treated to CM from respective cancer cells, and day 4 (D4) untreated and unconditioned medium (UC) day 6 (D6) myotubes. Myotubes immunostained with anti-myosin heavy chain (MyHC) and nuclei with DAPI. The Scale bar is 100 μm. **C)** Quantification of myotube diameter with comparison of the mean of all conditions relative to the mean of D6 control (uM), n=3. **D)** Quantification of MyHC precent area (%) of n=3. Data quantification for **C)** and **D)**: data are presented as mean ± SEM from n = 3 independent experiments. One-way ANOVA followed by Dunnett's multiple comparisons test against the D6 control group were used to determine statistical significance. *p < 0.05, **p < 0.01, ***p < 0.001, ****p < 0.0001, ns = not significant. **E)** Western blot validation of C/EBPβ expression in 7 murine cancer cell lines. Cyclophilin B (CYPB) is a loading control. **F)** Quantification of C/EBPβ (LAP isoform) expression. Data is presented as the mean ± SEM, n=3.

In culture, the most atrophic cancer cell line is B16, despite its lower levels of C/EBPβ expression. However, most cancer cell lines still express C/EBPβ except for ID8. Interestingly, ID8 expresses negligible amounts of C/EBPβ, and also has the highest myotube diameter, indicating that like EL4, this cancer cell line may be non-atrophic in culture. Thereby, for further validation the tumour cell lines should be inoculated in mouse models to confirm whether muscle wasting is occurring or not.

Thus, this analysis reveals additional models of atrophy and provides further support that C/EBPβ expression correlates with the ability to drive atrophy. These atrophic and non-atrophic models can therefore be used to determine a C/EBPβ-regulated gene signature.

4.1.2 Concentration and sizes of EVs in atrophic and non-atrophic in vitro models

EVs were collected and isolated from 7 murine cancer wildtype cell lines: LLC, MC38, B16, GL261, CT2A, ID8, and EL4 following the established protocol from the Burger lab.

Following EV isolation, nanoparticle tracking analysis (NTA) was conducted to assess EV size (nm) and concentration of particles normalized to protein content (particles/ug).

The nanoparticle results reveal the median size and average concentration of EVs (Figure 2 A, B). The highest concentration of EVs is observed to be secreted by B16, with the lowest concentration secreted by LLC. However, one-way ANOVA demonstrates that there is no significant difference in concentration of the EVs across the 7 cancer cell lines. Whereas the relative sizes of the EVs are different among the cancer cell lines. MC38, ID8, and EL4 have larger sized EVs when compared to B16, and CT2A. LLC and GL261 are not significantly different from the other cancer cell lines. Interestingly, the cell lines with smaller derived EVs, MC38, ID8 and EL4, are all considered to be non-atrophic (Figure 1. C). This data provides potential insight on their roles, as they carry information on the cell types they have been secreted from[56].

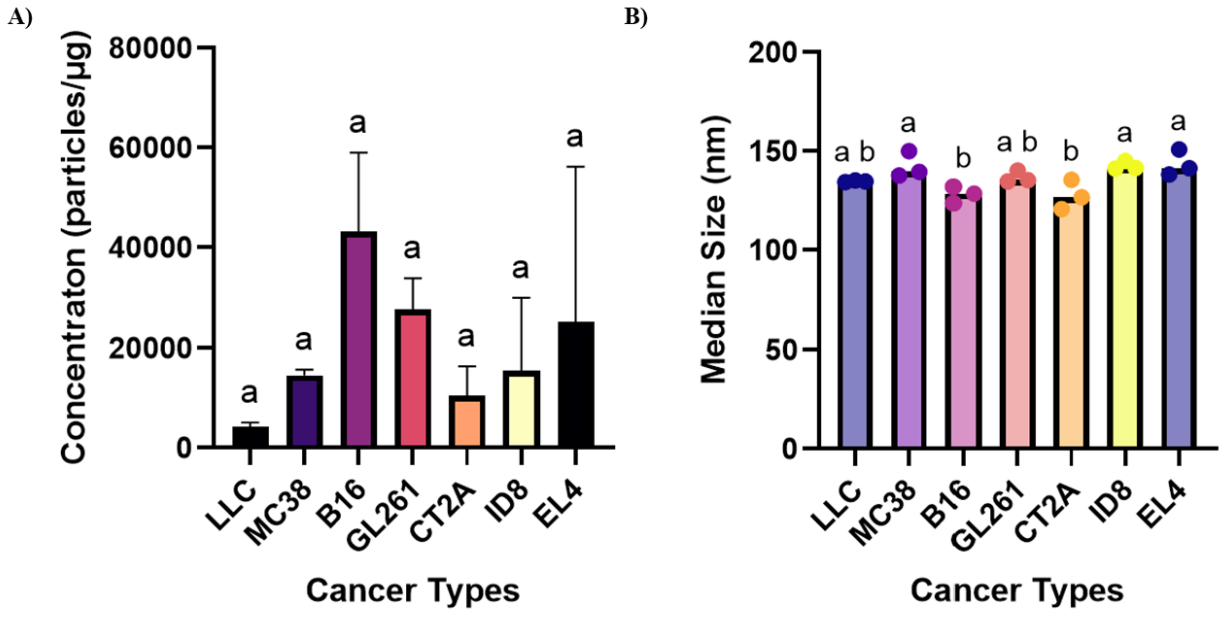

Figure 2. Average concentration and median size of EVs. A) Average concentration (particles/ug) of EVs, n =3. B) Median size (nm) of EVs, n=3. Data are presented as the mean ±

SEM. Different letters above bars indicate statistically significant differences at a cut-off of $p < 0.05$, as determined by one-way ANOVA followed by Tukey's multiple comparisons test.

4.1.3 LLC derived EVs and apoptotic bodies contribute to atrophy in vitro

As previously described, CM experiments (Figure 1A) were conducted to determine whether EVs directly contribute to atrophy, as indicated by a reduction in myotube diameter relative to D6 control myotubes. C2C12 myotubes were exposed to extracellular vesicles (EVs) and apoptotic bodies isolated from LLC wild-type (WT) cell lines. Treatment conditions included an untreated control cultured in unconditioned media (UC; Day 6, D6), CM derived from LLCs, EV- and/or apoptotic body-depleted CM, and direct treatment with isolated EVs or apoptotic bodies. All treatments were administered in a 1:1 ratio of differentiation media (DM) to CM (Figure 3-4. A, B)

LLC WT derived EVs demonstrate their ability to induce atrophy as observed by decreases in myotube diameter relative to day 6 controls (Fig 3. B). When EVs were completely removed from the CM (EV-free CM) there was no change in myotube diameter when compared to D6 controls (Fig 3. B). This indicates that LLC derived EVs play a significant role in causing the atrophic phenotype observed *in vitro*, and that removal of EVs from CM has a slight trend towards rescue of myotube size. Additionally, western blots staining for CD9 positively confirm the presence of LLC derived EVs, and the absence of expression of Calnexin serves as a negative control confirming the EVs isolated are pure with no contamination of cellular debris or organelles (i.e. ER fragments) (Figure 3. C).

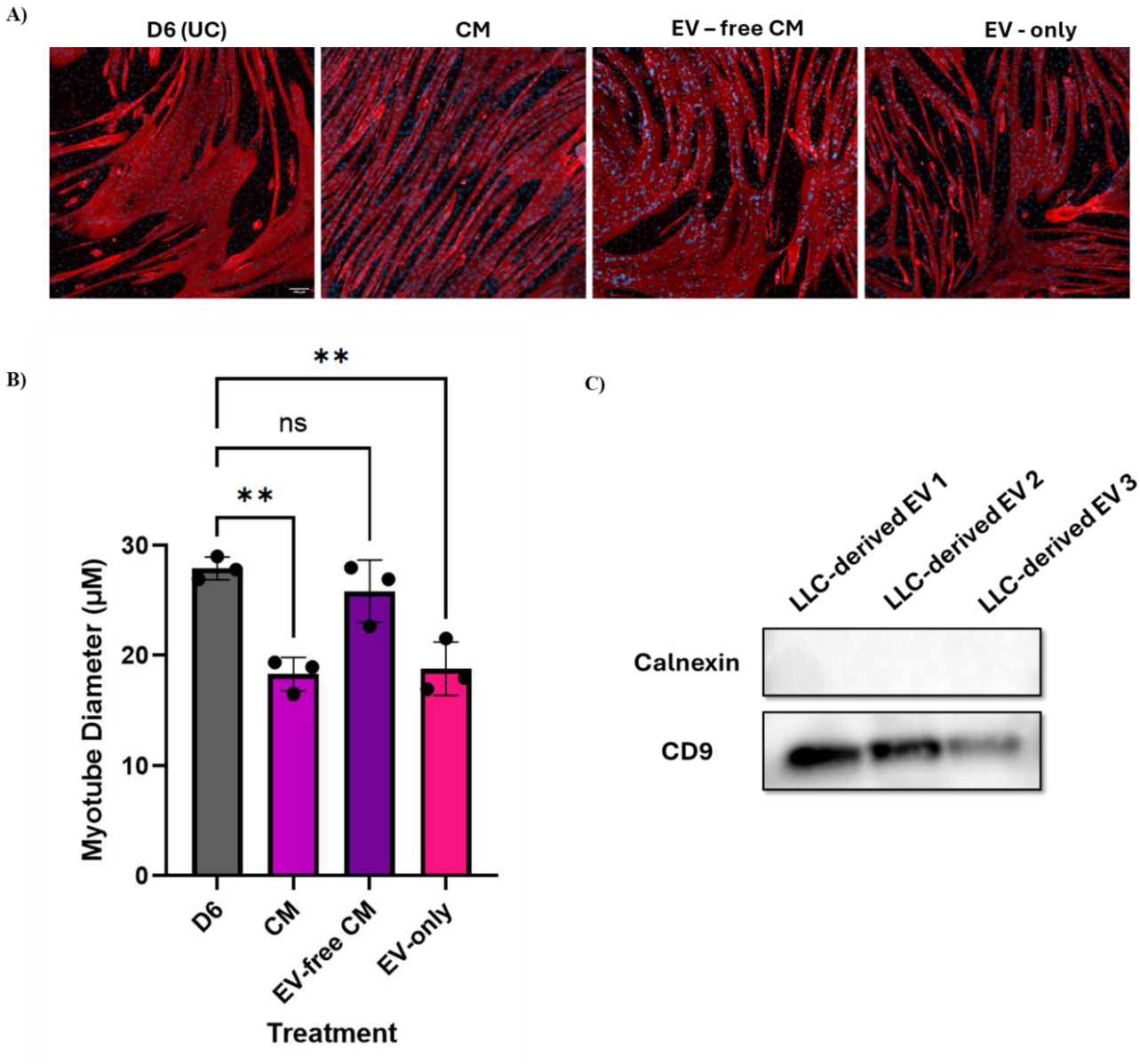

Figure 3. LLC derived EVs are critical for myotube atrophy in vitro. A) Immunofluorescence images of day 4 myotubes treated for two days to day 6 (D6) with a 1:1 ratio CM-, EV free CM-, or EVs to DM from LLC WT, and unconditioned medium (UC) day 6 myotubes. Myotubes immunostained with anti-myosin heavy chain (MyHC) and nuclei with DAPI. The Scale bar is 100 µm. **B)** Quantification of myotube diameter (uM) with comparison of the mean of all conditions relative to the mean of D6 control, n=3. Data is presented as the mean ± SEM. Statistical analysis was performed using one-way ANOVA followed by Dunnett's multiple comparisons test with D6 as the control group. $p < 0.01$ is considered significant (**). Comparisons to EV-free CM were not significant (ns), while both CM and EV-only conditions were significantly different from D6. **C)** Western validation of presence of LLC WT derived EVs via staining of calnexin and CD9 antibodies.

Additionally, given that apoptotic bodies may also be contributing to the atrophic phenotype *in vitro* they were also investigated (Figure 4. A, B). C2C12 myotubes were treated with CM, apoptotic body-depleted CM (Apo-free CM), or isolated apoptotic bodies (Apo) and compared to untreated differentiation controls (D4 and D6) (Fig 4. A, B) in a 1:1 ratio of DM to CM treatment (i.e. CM, Apoptotic body free CM, apoptotic bodies). LLC WT derived apoptotic bodies demonstrate their ability to induce atrophy as observed by decreases in myotube diameter relative to day 6 controls (Figure 4. B).

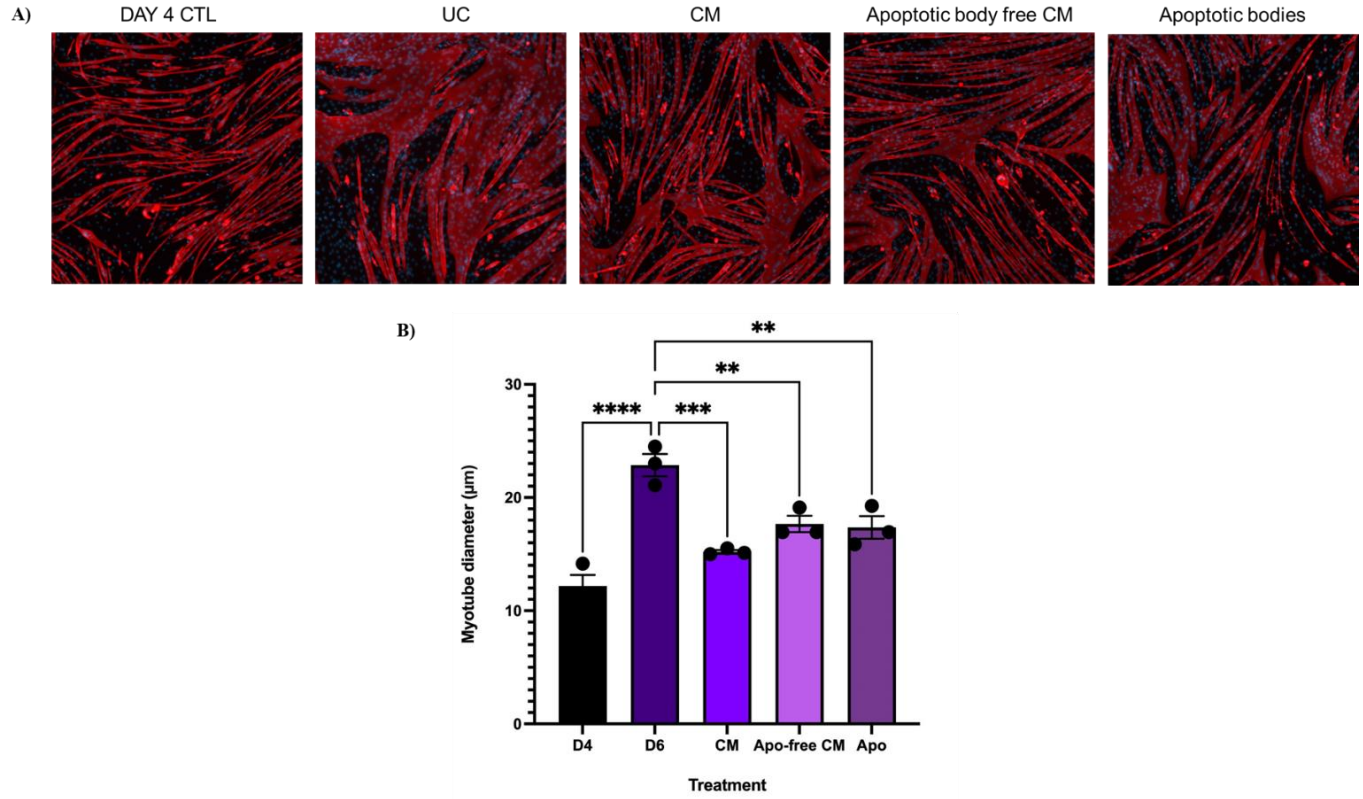

Figure 4. LLC derived apoptotic bodies contribute to atrophy *in vitro* A) Immunofluorescence images of day 4 myotubes treated for two days to day 6 (D6) with a 1:1 ratio CM-, apoptotic bodies free CM-, or apoptotic bodies to DM from LLC WT, and day 4 (D4) untreated and unconditioned medium (UC) day 6 myotubes. Myotubes immunostained with anti-myosin heavy chain (MyHC) and nuclei with DAPI. The Scale bar is 100 µm. **B)** Quantification of myotube diameter (uM), n=3. with comparison of the mean of all conditions relative to the mean of D6 control. Data is presented as the mean ± SEM. Different letters above bars indicate statistically significant differences at a cut-off of $P < 0.05$ (one-way ANOVA) followed by Tukey's multiple comparison test.

4.1.4 EVs derived from MC38 and EL4 do not cause atrophy in vitro

The previously described CM experiments (Figure 1. A) were conducted with MC38 WT and EL4 WT EVs. Extracellular vesicles (EV) were isolated from MC38 WT and incubated with C2C12s to determine if they could induce atrophy (Figure 5. A, B). There are no statistical differences between the treatments (CM, EV-free CM, EV) and the D6 control (see Figure 5. B)) indicating that MC38 derived EVs have no role in inducing atrophy *in vitro*. Western blot staining confirms the presence of MC38 derived EVs via CD81, and calnexin serves as a negative control for overall purity (Figure 5. C).

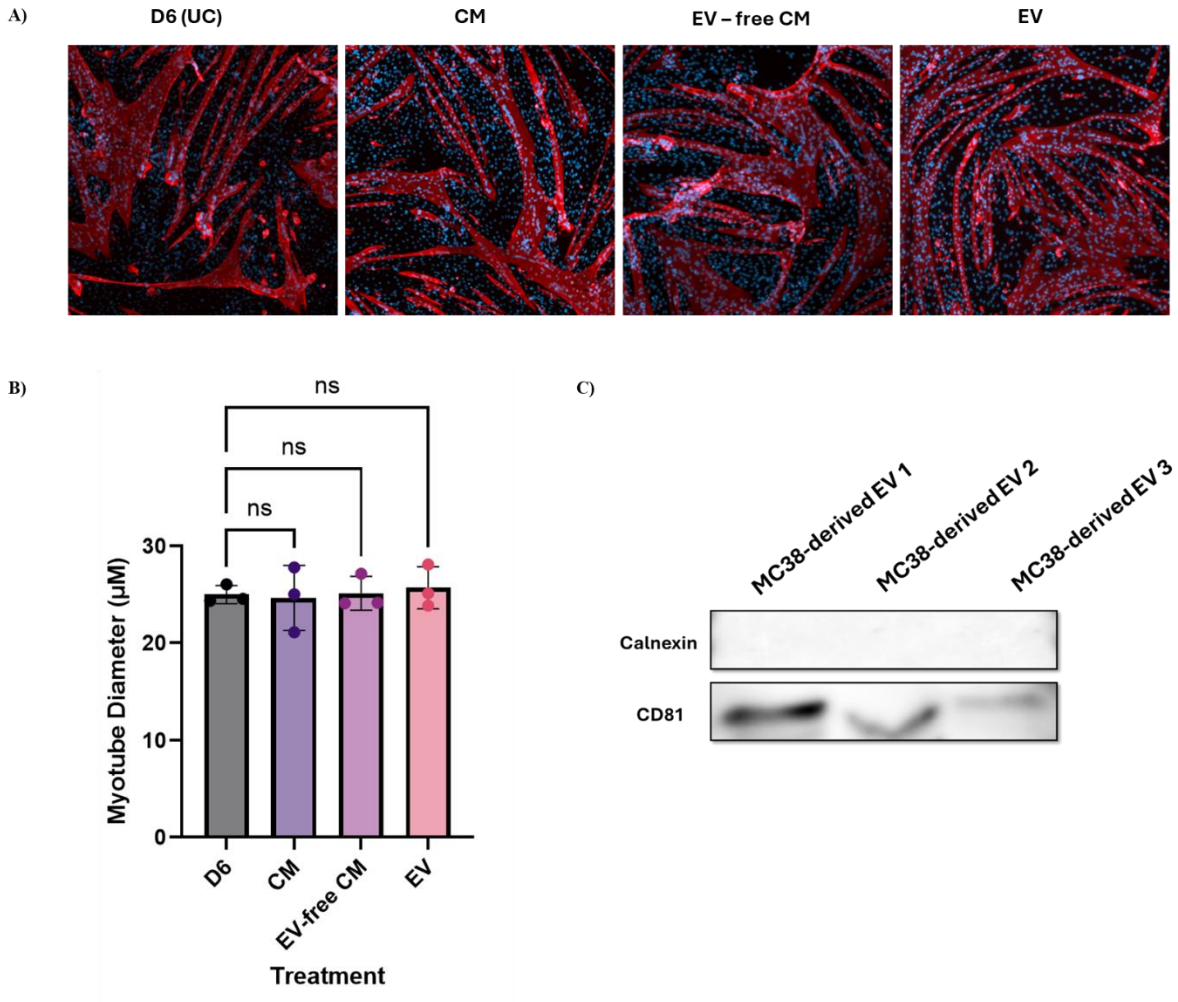

Figure 5. MC38 derived EVs do not cause atrophy *in vitro*. A) Immunofluorescence images of day 6 myotubes treated to CM from MC38 WT, and day 4 (D4) untreated and unconditioned medium (UC) day 6 myotubes. Myotubes immunostained with anti-myosin heavy chain (MyHC) and nuclei with DAPI. The Scale bar is 100 μm. **B)** Quantification of myotube diameter (uM), n=3 with comparison of the mean of all conditions relative to the mean of D6 control. Data is presented as the mean ± SEM. Statistical analysis was performed using one-way ANOVA followed by Dunnett's multiple comparisons test with D6 as the control group. No statistically significant differences were observed between D6 and any of the treatment groups (CM, EV-free CM, or EV-only); all comparisons were not significant (ns, $p > 0.05$). **C)** Western validation of presence of MC38 WT derived EV's via staining of calnexin and CD81 antibodies.

The same experiment was conducted with EL4 isolated extracellular vesicles (EVs). EVs were isolated and incubated with C2C12s to determine if they could induce atrophy (Figure 6. A, B). There are no statistical differences between the treatments (CM, EV-free CM, EV) and the D6 control (see Fig 6. B)) indicating that EL4 derived EVs have no role in inducing atrophy *in vitro*. Western blot staining also confirms the presence of EL4 derived EVs via CD81, and calnexin serves as a negative control for overall purity (Figure 6. C)

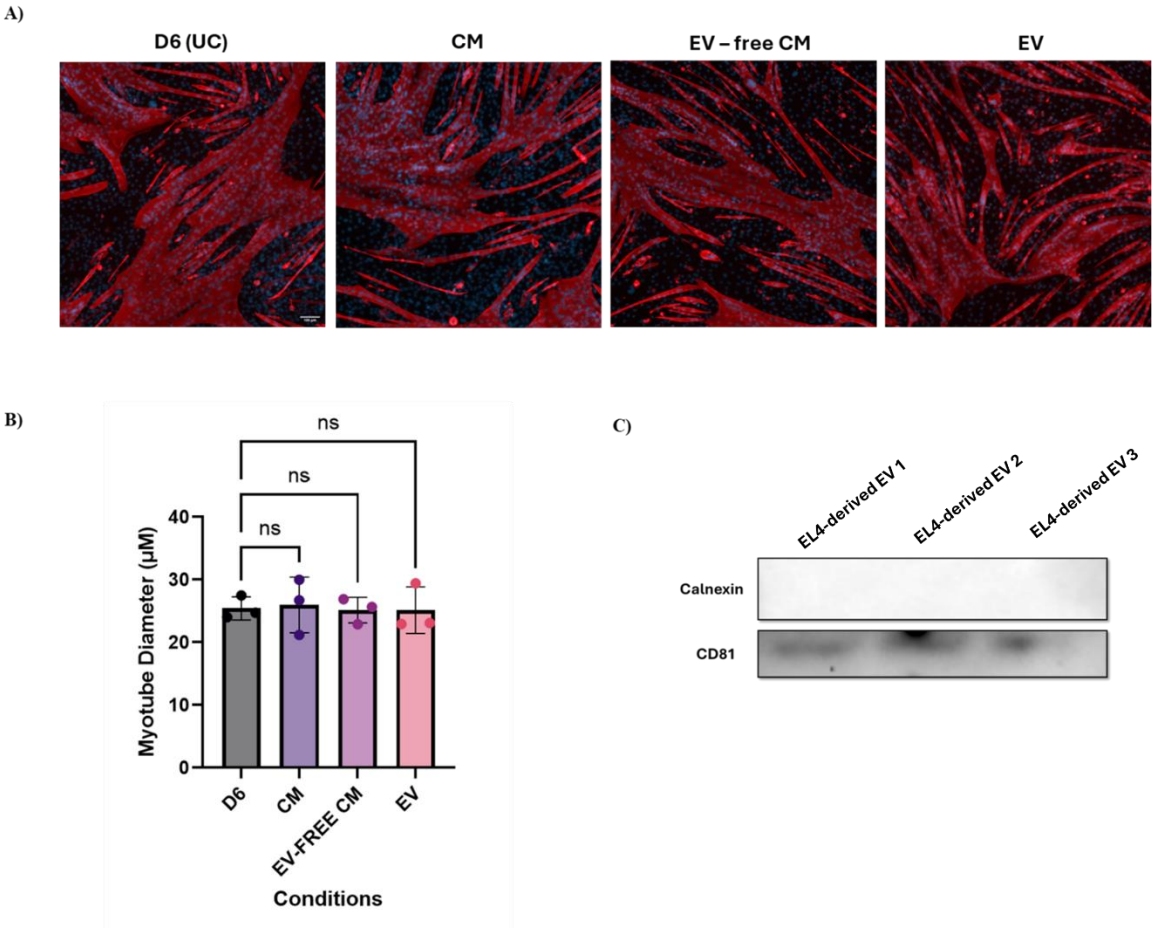

Figure 6. EL4 derived EVs do not contribute to atrophy *in vitro*. A) Immunofluorescence images of day 6 (D6) myotubes treated with MC38 WT condition medium (CM), EV-free CM, and EVs, and untreated unconditioned medium (UC) day 6 myotubes. Myotubes immunostained with anti-myosin heavy chain (MyHC) and nuclei with DAPI. The Scale bar is 100 μm. **B)** Quantification of myotube diameter (uM), n=3 with comparison of the mean of all conditions relative to the mean of D6 control. Data is presented as the mean ± SEM. Statistical analysis was conducted using one-way ANOVA followed by Dunnett's multiple comparisons test with D6 as the control group. No statistically significant differences were observed between D6 and any of the treatment groups (CM, EV-free CM, or EV-only); all comparisons were not significant (ns, $p > 0.05$). **C)** Western validation of presence of EL4 WT derived EV's via staining of calnexin and CD81 antibodies.

4.2 Aim 2: Develop a TurboID-based system to label and identify secreted proteins in a cachexia-inducing cancer model, and link identified proteins to C/EBPβ-dependent gene expression changes.

Cancer cachexia secretome is very difficult to study *in vitro*[47], in part due to the multitude of contaminants in serum that affect the purity of MS read outs[48]. For this reason, enzymatic

biotinylation is a promising tool that allows for proximity labeling of proteins and EVs in the ER[57–59]. This technique *in vitro* enables the differentiation between factors secreted by the tumours and contaminants within the serum[60,61], and *in vivo* differentiation between tumour-derived factors and host-derived factors[62,63]. The use of enzymatic biotinylation is a tool that will enable more insight on the mechanisms involved in inducing muscle atrophy and the potential signalling pathways involved in cancer cachexia.

4.2.1 Validation of successful intracellular integration of TurboID in 7 murine cancer cell line constructs

The biotin ligase selected for the tagging of proteins was a TurboID construct that selectively localizes to the ER membrane of mammalian cells. TurboID was selected over other biotin ligases (ie BioID) given its faster rate of biotinylating proteins (10 mins), high efficiency, low toxicity, and better suited for in vivo settings[4,64]. To stably express the promiscuous ER-resident mutated BirA enzyme on the cancer cell lines, I used the C1(1-29)-TurboID-V5_pLX304 plasmid (Addgene #107175).

This plasmid was chosen as it is a lentiviral vector enabling the stable and long-term integration into DNA and contains an ER-localized promiscuous biotin ligase (BirA) allowing for the tagging of proteins as they are produced. The plasmid DNA was isolated and verified via restriction digest (Figure. 7 A). Following verification of the DNA sequence, lentivirus was created and collected and then transduced into target cells followed by selection with antibiotics, allowing for the stable selection of cancer cell lines with TurboID (Fig. 7. B – E). These seven murine cancer cell lines included cell lines wildtype (WT), gain of function (GOF), and loss of function (LOF) C/EBPβ models. WT lines were LLC and MC38. GOF models were LLC cell lines transduced to overexpress C/EBPβ denoted as LLC C/EBPβ, with control empty vector

(pLX) denoted as LLC pLX. LOF models included LLC and MC38 cell lines with a CRISPER KO of C/EBPβ, denoted as LLC- or MC38-sg3, and control vector for the KO denoted as LLC- or MC38-sgCTL. The OE and KO models were created by A. Saleh (unpublished) in accordance with the wildtype expression levels of C/EBPβ of LLC and MC38 WT cell line (Figure 1. F).

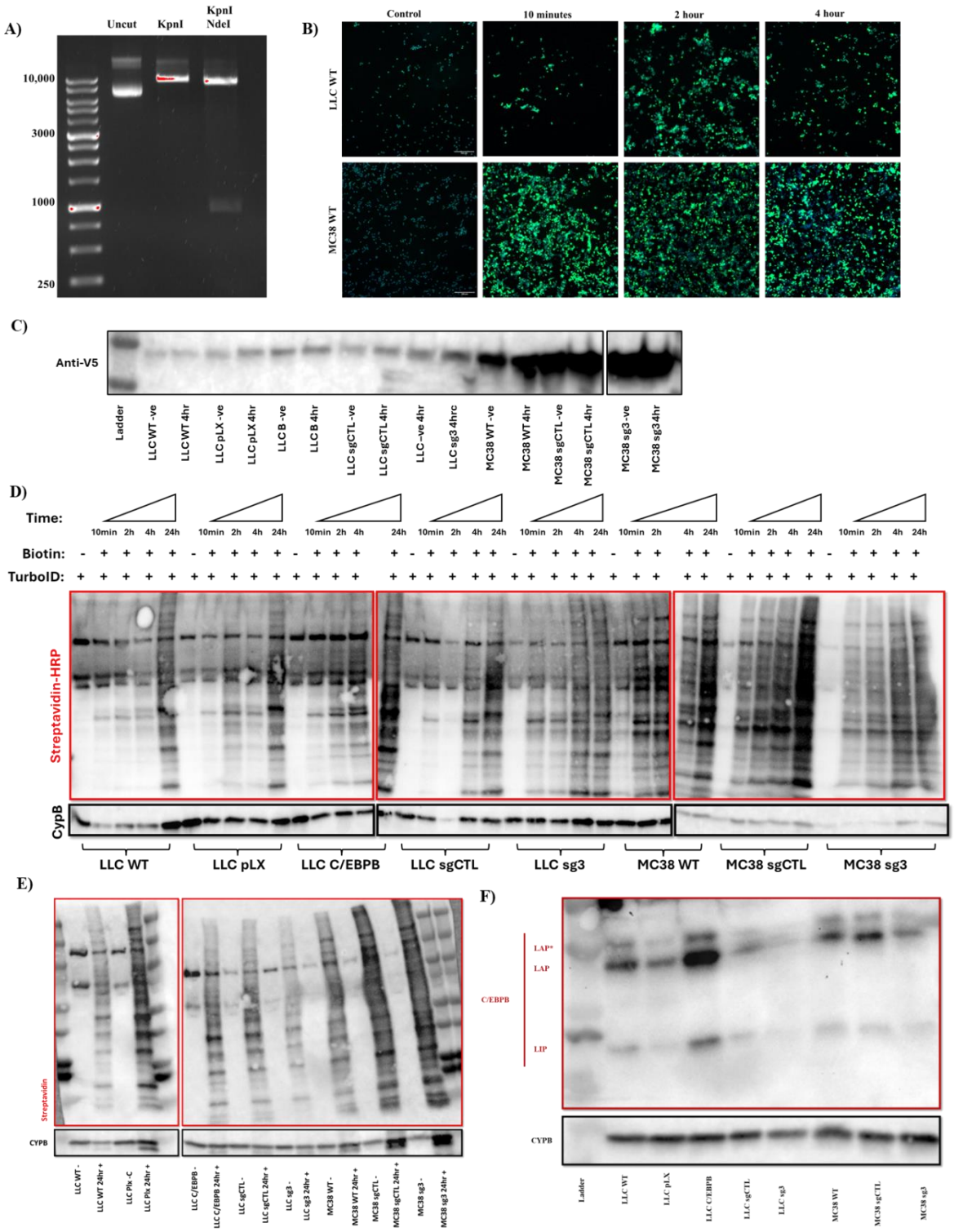

Figure 7. Validation of TurboID vector transfection into seven murine cancer cell line constructs. A) Restriction digest confirming correct isolation of plasmid DNA. **B)** Immunofluorescence images of LLC WT and MC38 cancer cell lines stably expressing ER-resident TurboID incubated in the absence (control) and presence of 50 µM exogenous biotin for 10 minutes, 2 hours, and 4 hours. Cancer cells immunostained with AF488 (Alexa fluro 488)

Streptavidin and DAPI for nuclei **C)** Cancer cell line constructs integrated with TurboID vector where exposed to no exogenous biotin (-ve) or exposed to 50 μM of exogenous biotin for 4 hours. Anti-V5 blotting detects ligase expression indicating integration of TurboID vector 7 cancer cell line constructs **D)** Time course experiment and comparison of TurboID activity across 7 cancer cell lines. 50 μM of exogenous biotin was used for labelling with the following incubation intervals: 10 minutes, 2 hours, 4 hours, and 24 hours. Streptavidin-HRP detects promiscuously biotinylated proteins. Biotin added (+) and no exogenous biotin added (-) **E)** Streptavidin-HRP detects promiscuously biotinylated proteins with presence and absence (-) of 50 μM exogenous biotin with a 24-hour incubation timeline. **F)** Western blot validation C/EBPβ expression in 7 cancer cell line constructs (WT/GOF/LOF models). Cyclophilin B (CYPB) is a loading control.

Cancer cell lines were grown and incubated with 50 μM of exogenous biotin to confirm successful labelling of proteins and incubated with no biotin as a control. Immunofluorescence images confirm the activity of TurboID via presence of green fluorophore (AF188) attached to Streptavidin in LLC and MC38 WT cell lines stably expressing TurboID (Fig 7. B). Furthermore, immunoblotting for anti-V5 confirms the integration of TurboID across the 7 cancer cell lines as it detects ligase expression in presence and absence of exogenous biotin (Fig 7. C). Immunoblotting for streptavidin-HRP which binds to biotin, confirms the presence of biotinylated proteins as evidenced by the banding pattern observed in the presence of exogenous biotin, whereas in the absence of biotin no banding pattern is observed (Fig 7. D). Furthermore, MC38 WT and KO models appear to have more efficient TurboID activity than LLC WT and KO/OE models based on the high expression of Streptavidin (Fig 7. D).

Generally, more biotinylated proteins are observed with longer incubation times of exogenous biotin for all 7 cancer cell line constructs (Fig 7. D). This increase in activity may be attributed to higher enzymatic activity and/or non-specific binding. Interestingly, LLC knockdowns of C/EBPβ appear to have the weakest expression in terms of biotinylated proteins when compared to the other constructs (Fig 7. E). This potentially could indicate that there are less secreted/membrane bound proteins produced when C/EBPβ is knocked down. All 3 of the

MC38 constructs appear to have very high enzymatic activity with many proteins tagged with biotin (Fig 7. E). Furthermore, the overall expression levels of C/EBPβ are confirmed and validated for all 7 cancer cell lines including WT, GOF, and LOF models after stable integration of TurboID vector (Fig 7. F). Thereby, these results indicate the successful integration of the TurboID vector into all 7 cancer cell lines and confirm activity of TurboID in the presence of exogenous biotin.

4.2.2 Validation of secretion of biotin-tagged proteins and streptavidin-enrichment capture

To assess the capture of secreted proteins, cell lines with the stable integration of ER-localized TurboID vector were grown in growth media (GM) for 2 days (48 hours) with addition of exogenous of biotin or in the absences of biotin (control), followed by 2 days (48 hours) in normal GM (Figure 8. A) and conditioned media (CM) was collected on day 4. Immunoblotting of Streptavidin-HRP was conducted on the 7 cancer cell line constructs expressing the TurboID vector conditioned media (CM) (Fig 8. B). Immunoblotting of streptavidin-HRP revealed the presence of secreted proteins in the presence of exogenous biotin, and absence of secreted proteins in the absence of exogenous biotin (Fig 8. B). Moreover, no proteins are detected in the unconcentrated (CM) samples, indicating that the conditioned media will need to be concentrated for secreted protein detection (Fig 8. B). This validation indicates that the seven murine cancer cell lines stably expressing the TurboID vector, can be used *in vitro* and potentially *in vivo* to study tumour specific secreted proteins, which could be used further to reveal communication networks by assessing protein trafficking and uptake.

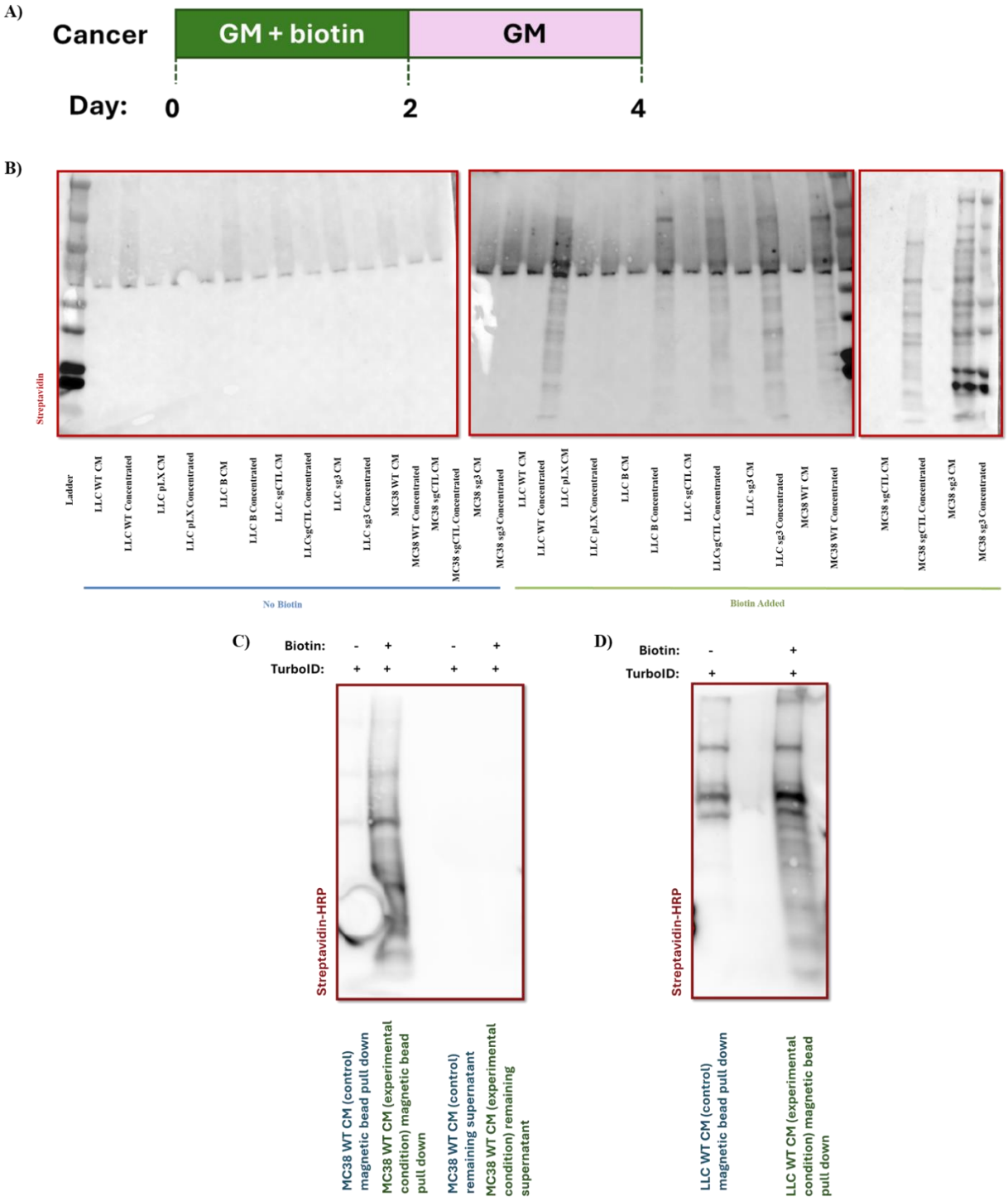

Figure 8. Validation of secreted biotin enriched protein capture. A) Schematic representation of method for secreted protein isolation following timeline used in conditioned medium (CM) experiments when collecting CM. Cancer cell line constructs with integrated ER localized TurboID vector are grown for 2 days in growth media with the addition of 50 µM of exogenous biotin or absence of 50 µM exogenous biotin. Following day 2, media change is performed with the addition of new growth media (GM) on day 2. Cancer cells are grown till day 4 and CM is

collected on day 4. **B)** Cancer cell line constructs grown either in the presence (Biotin Added) or absence (No Biotin) of exogenous biotin in DMEM, and conditioned media collected is either unconcentrated (CM) or concentrated via Amicon filters. Immunoblotting of Streptavidin-HRP detects promiscuously biotinylated proteins in conditioned media that is unconcentrated (CM) or concentrated via Amicon filters. **C)** Streptavidin-HRP blotting for proteins secreted form MC38 WT cell lines grown in the presence (green) or absence (blue) of exogenous biotin and then isolated via streptavidin coated magnetic beads and remaining supernatant. **D)** Streptavidin-HRP blotting for proteins secreted form LLC WT cell lines enriched via magnetic beads in the presence (green) and absence (blue) of exogenous biotin.

The experiment was conducted again (Fig 8. A) but with the use of streptavidin magnetic bead enrichment to isolate secreted proteins from the conditioned media (Fig 8. C, D). Conditioned media was collected from LLC WT and MC38 WT expressing TurboID vector, concentrated via Amicon filters, and incubated with streptavidin coated magnetic beads at 4°C overnight (O/N) on shaker. Using streptavidin magnetic beads capture, secreted proteins that were tagged with biotin were isolated and confirmed via immunoblotting of Streptavidin-HRP as seen by the smear and/or banding pattern observed of proteins with different sizes detected (Fig 8. C, D). Whereas cancer cell lines grown in the absence of biotin do not indicate the presence of proteins as no proteins are detected (Fig 8. C, D). Additionally, the remaining supernatant (i.e., the conditioned media after removal of magnetic beads bound to biotinylated proteins) shows no detectable signal, indicating that the magnetic beads successfully captured all tagged proteins (Fig 8. C). However, higher background is seen in LLC WT controls (i.e absence of exogenous biotin) when compared to MC38 WT controls (Fig 8. C, D).

Thus, these results confirm the successful capture of secreted proteins promiscuously tagged by TurboID. Furthermore, this technique's ability to selectively isolate secreted proteins highlights its novelty, as it enables differentiation from serum-derived or contaminant proteins and holds strong potential for *in vivo* applications to uncover key intercellular communication networks in cancer cachexia.

4.2.3 LLC WT with integrated TurboID vector derived CM causes atrophy in vitro

To assess whether TurboID integration affects the atrophic phenotype *in vitro* of the LLC WT cell line, conditioned media experiments were conducted (Figure 9. A - C). As previously described, LLC WT with the TurboID vector were either grown in the presence or absence of exogenous biotin (Fig 9. A) for 48 hours, followed by a media change and the collection of conditioned media 48 hours later (day 4). C2C12s were then treated with CM for 48 hours in a 1:1 ratio of CM to differentiation media (DM) (Fig 9. A).

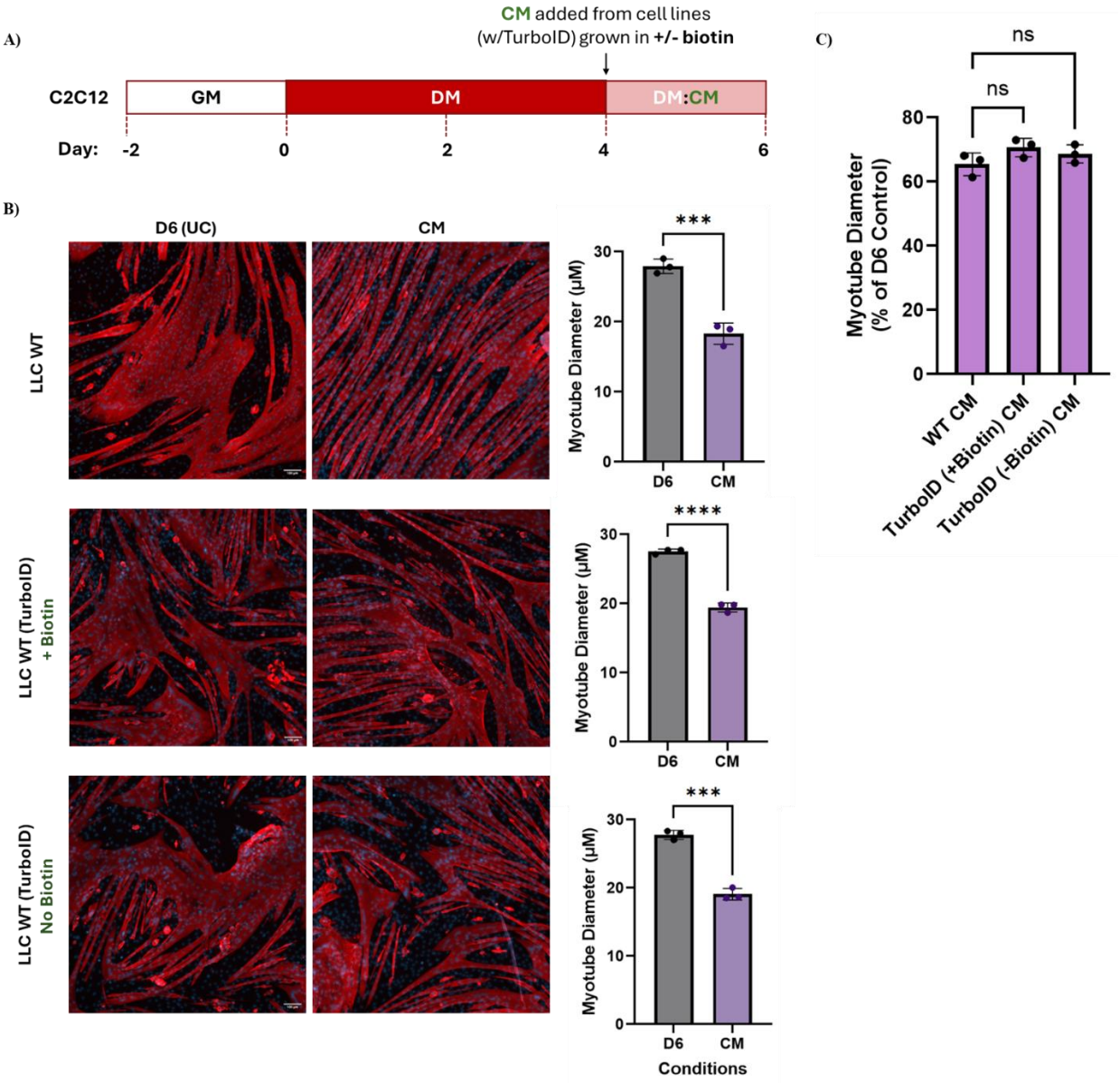

Figure 9. Cancer conditioned medium (CM) experiment of LLC WT with TurboID vector
A) Schematic representation of the experimental workflow. C2C12 myoblasts were cultured to confluency in growth media (GM) and subsequently differentiated in low-serum differentiation media (DM) for 4 days (D4). In parallel, cancer cells were grown to confluency in GM for 2 days either in the absence or presence of exogenous biotin, after which the media was replaced to collect conditioned media (CM). On Day 4 (D4), differentiated myotubes were treated for an additional two days (until Day 6, D6) with a 1:1 mixture of conditioned media (CM) and fresh differentiation media (DM) for experimental conditions, or a 1:1 mixture of DM and growth media (GM) for controls. B) Immunofluorescence images of day 6 (D6) myotubes treated to CM from LLC WT, and LLC WT with TurboID grown in the presence or absence of biotin and unconditioned medium (UC) day 6 (D6) myotubes. Myotubes immunostained with anti-myosin heavy chain (MyHC) and nuclei with DAPI. The Scale bar is 100 µm. Data quantification for (LLC WT): Data are presented as the mean ± SEM. An unpaired two-tailed t-test comparing D6 and CM revealed a statistically significant reduction in the CM group (***, p = 0.0008). n = 3

per group. Data quantification for (LLC WT TurboID + Biotin): Data are presented as the mean ± SEM. Statistical comparison between D6 and CM was performed using an unpaired two-tailed t-test. A highly significant difference was observed (****, $p < 0.0001$), with CM showing reduced signal relative to D6. n = 3 per group. Data quantification for (LLC WT TurboID No Biotin): Data are presented as the mean ± SEM. An unpaired two-tailed t-test comparing D6 and CM revealed a statistically significant reduction in the CM group (***, $p = 0.0001$). n = 3 per group. **C)** C2C12 myotubes were treated with CM derived from either TurboID or wild-type LLC cells. Myotube diameter was measured on Day 6 and normalized to untreated Day 6 (D6) controls within each experiment. Data are presented as the mean ± SEM. A one-way ANOVA followed by Dunnett's post hoc test revealed no statistically significant differences between WT CM and TurboID (+Biotin) or (-Biotin) CM (ns, $p > 0.05$). n = 3 per group.

CM derived from LLC WT with TurboID vector incubated in the presence or absence of exogenous biotin causes a significant decrease in myotube diameter (uM) (Fig 9. B – C). Additionally, to determine whether TurboID integration alters the cachectic effect of LLC WT derived conditioned media (CM), myotube diameters were measured and normalized to untreated Day 6 (D6) controls for both TurboID and wild-type (WT) conditions (Fig 9. C). Normalization enabled direct comparison of the relative degree of myotube atrophy induced by CM from each cell line. While both TurboID-CM and WT-CM significantly reduced myotube diameter relative to their respective D6 controls (Fig 9. B), no statistically significant difference was observed between the TurboID-CM conditions when compared to WT-CM (Fig 9. C). These findings suggest that the CM derived from LLC WT cell lines expressing TurboID does not affect their ability to induce myotube atrophy *in vitro*, and that the cell lines cause the same level of atrophy when compared to WT conditions.

4.2.4 Mass spectrometry data reveals the capture of novel secreted proteins

Given that the TurboID machinery has been confirmed to promiscuously tag proteins with biotin *in vitro*, and that the CM from LLC WT with the TurboID vector exert the same level of atrophy *in vitro*, we decided to use this method to explore the secretome of cachectic cancer cell line, LLC. Mass spectrometry was performed on the conditioned media (CM) of two control

samples and 3 experimental conditions conducted according to established protocols (Figure 10. A). The control samples were wild-type LLC grown in the presence of biotin (DP1142_1_TurboID) and TurboID LLC grown in the absence of biotin (DP1142_2_NoBiotin) (Fig 10. C). The experimental conditions were TurboID LLC grown in the presence of biotin as trial 1 [T1 (DP1142_3_T1)], trial 2 [T2 (DP1159_1_T2)], and trial 3 [T3 (DP1159_1_T3)] (Fig 10. C – D). Immunoblotting of Streptavidin-HRP was also conducted to ensure TurboID vector was active and tagging proteins intracellularly and capture of secreted proteins via streptavidin coated magnetic beads was successful (Fig 10. B).

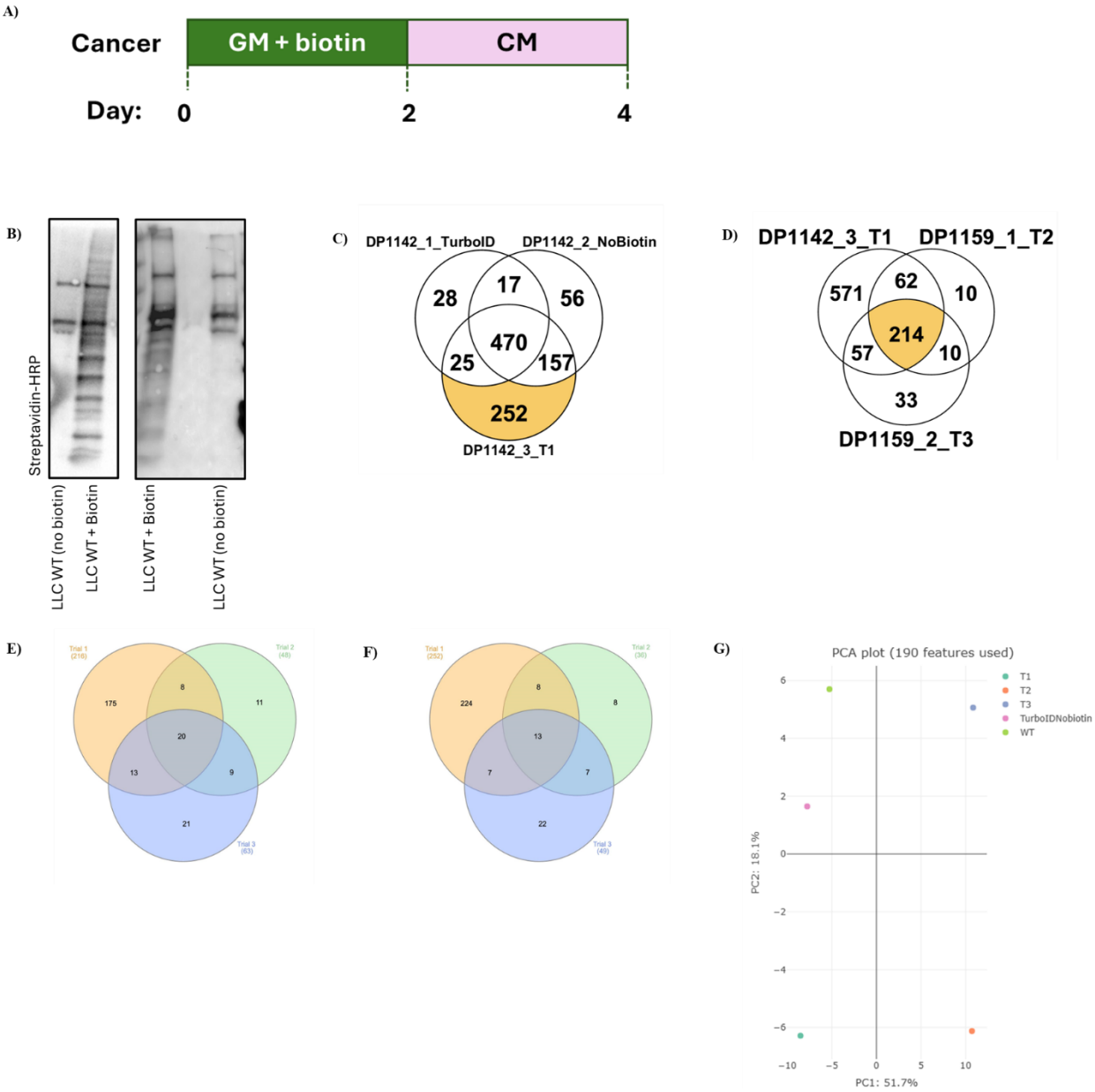

Figure 10. Mass spectrometry results of LLC WT secreted proteins. A) Schematic representation of method for secreted protein isolation following timeline used in conditioned medium experiments when collecting conditioned media. Cancer cell line constructs with integrated ER localized TurboID vector are grown for 2 days in growth media (GM) with the addition of 50 µM of exogenous biotin or absence of 50 µM exogenous biotin. Following day 2, media change is performed with the addition of new growth media (GM) for 2 days to day 4. Conditioned media (CM) is collected on day 4. **B)** Streptavidin-HRP blotting for proteins tagged intramedullary (blot on right) and secreted proteins form LLC WT cell lines enriched via magnetic beads in the presence and absence of exogenous biotin (blot on left). **C)** Proteins identified in controls (DP1142_2_NoBiotin and DP1142_3_T1) and Trial 1 experimental condition (DP1142_3_T1). **D)** Proteins identified in Trial 1, 2, and 3 before removal of

contaminant and background proteins. **E) & F)** Proteins identified in common between experimental condition trial 1, 2, and 3. after removal of background and contaminant proteins using Scaffold software (**E)**) and Fragpipe software (**F)**) with minimum of 2 peptide thresholds and 1.0% FDR cut-off. **G)** PCA plot demonstrating feature differences and likeness between controls and experimental conditions

Mass spectrometry data from LLC WT secreted proteins, confirmed the ability to capture novel proteins as 252 unique proteins were captured in the presence of biotin (Trial 1: DP1142_3_T1) in comparison to controls which captured 56 (DP1142_2_NoBiotin) and 28 proteins (DP1142_1_TurboID) (Fig 10. C). Trial 1 to 3 initially revealed 214 proteins in common without removal of background/contaminant proteins (Figure 10. D). Following removal, 24 uniquely secreted proteins were found (n=3) (Table 1) by analyzing and combining the proteins observed in the Scaffold software and Fragpipe software (Fig 10. E, F).

Although Trial 1 captured a higher number of unique proteins compared to Trials 2 and 3, this is likely due to increased cell lysis, as evidenced by the presence of proteins found in Trial 1 and controls. Additionally, intracellular housekeeping proteins such as Cyclophilin β (Peptidyl-prolyl cis-trans isomerase B) were found both in the experimental (T1) and control conditions. In contrast, Trials 2 and 3 did not exhibit these housekeeping proteins and nuclear localized proteins, suggesting reduced cell lysis and a more specific capture of secreted or membrane-associated proteins. Additionally, proteins like BCL2L13, PDCD6IP, and HYOU1 were found in Trial 1 and controls, but not in Trial 2 and 3, further indicating increased cell lysis in Trial 1 and controls as BCL2L13 is pro-apoptotic, PDCD6IP is linked to apoptosis signalling, and HYOU1 is upregulated in hypoxic conditions to protect from stress. This further indicates that the disparities observed in the number of proteins identified in Trial 1 and controls when compared to Trial 2 and 3, have to do with increased cell lysis in the proteomic preparation.

Cell lysis and debris further accounts for the differences observed in the PCA plot where the controls (TurboID-NoBiotin and WT) are grouped together along PC1 indicating more similar features accounting for contaminants such as KERATIN (Fig 10. F). T2 and T3 are grouped together along both PC1 and PC2 indicating features that are more alike (Fig 10. F). However, T1, T2, and T3 are quite distinct from the controls (TurboID-NoBiotin and WT) which indicates that T1, T2, and T3 contain secreted proteins that were captured via their biotin labels. T1 is distinct from both T2 and T3 which is due to higher amounts of lysis in sample preparation for T1 as discussed above. Additionally, T1 and the controls were prepared and sent for MS analysis earlier, while T2 and T3 were prepared on a different date.

Between T1, T2, and T3 twenty-four proteins were identified (Table 1). These proteins range from the smallest protein identified being 12 kDa to the largest protein identified as 233 kDa (Table 1). This indicates the wide range of proteins that were tagged with biotin by TurboID, secreted out of the cell, and isolated via the streptavidin coated magnetic beads. Moreover, almost all the proteins are found on Vessiclepedia, indicating that the have been derived from a variety of extracellular vesicles (EVs), with the exception of SRPRA.

Table 1. Summary of the 24 proteins identified from all 3 trials. The table lists proteins detected in the dataset along with their UniProt ID, alternate gene/protein identifiers, molecular weight (kDa), and associated Vesiclepedia ID. The asterix (*) represents a protein that is part of the Top 100 EV protein list on Vesiclepedia.

UniProt ID	Alternate ID	Molecular Weight	Protein Name	Vesiclepedia ID
P10639	TXN	12 kDa	Thioredoxin	VP_22166
Q61029	Tmpo	50 kDa	Lamina-associated polypeptide 2, isoforms beta/delta/epsilon/gamma	VP_7112

Q9EQU5	Set	33 kDa	Protein SET	VP_56086
O08547	Sec22b	25 kDa	Vesicle-trafficking protein Sec22b	VP_310710
Q69ZN7	Myof	233 kDa	Myoferlin	VP_226101
Q9WV55	Vapa	28 kDa	Vesicle-associated membrane protein-associated protein A	VP_30960
Q5FWK3	Arhgap1	50 kDa	Rho GTPase-activating protein 1	VP_228359
Q91YH5	Atl3	61 kDa	Atlastin-3	VP_109168
Q61335	Bcap31	28 kDa	B-cell receptor-associated protein 31	VP_293852
P53986	Slc16a1	53 kDa	Monocarboxylate transporter 1	VP_57506
Q8VCF0	Mavs	53 kDa	Mitochondrial antiviral-signaling protein	VP_57506
O08579	Emd	29 kDa	Emerin	VP_2010
O55022	Pgrmc1	22 kDa	Membrane-associated progesterone receptor component 1	VP_291948
P27546	Map4	117 kDa	Microtubule-associated protein 4	VP_4134
P51125	Cast	85 kDa	Calpastatin	VP_831
Q01405	Sec23a	86 kDa	Protein transport protein Sec23A	VP_58817
Q3U9G9	Lbr	71 kDa	Delta(14)-sterol reductase LBR	VP_3930

Q61024	Asns	64 kDa	Asparagine synthetase [glutamine-hydrolyzing]	VP_27053
Q61249	Igbp1	39 kDa	Immunoglobulin-binding protein 1	VP_58845
Q62351	Tfrc	86 kDa	Transferrin receptor protein 1	VP_22042*
Q6PGH2	Jpt2	20 kDa	Jupiter microtubule associated homolog 2	VP_15374
Q8CIN4	Pak2	58 kDa	Serine/threonine-protein kinase PAK 2	VP_224105
Q99K01	Pdxdc1	87 kDa	Pyridoxal-dependent decarboxylase domain-containing protein 1	VP_23042
Q9DBG7	Srpra	70 kDa	Signal recognition particle receptor subunit alpha	N/A

The intensity values measure the signal strength of detected proteins, and the quantitative spectra counts reflect the number of times peptides from proteins are identified. In this case, the highest intensity detected is for TXN, TMPO, and LBR, whereas the lowest are CAST, IGBP1, and JPT2 (Figure 11. A). The spectra count reveals the highest counts as TXN, TMPO, and LBR, whereas lowest detected are MAP4, JPT2, and EMD (Fig 11. B). Interestingly, the highest detected are all different sized proteins, for example TXN is 12 kDA and LBR is 71 kDa, this highlights this technologies sensitivity of the TurboID mechanism to tag proteins of various sizes and therefore capture both small and large proteins.

Additionally, STRING annotation reveals predicted or known functional interactions between proteins (Fig 11. C). There are 3 main clusters of interactions shown: VAPA-BCAP31-LBR-EMD-TMPO, ATL3-SEC22B-SEC23A, and ARHGAP1-PAK2-TFRC. Experimentally

determined interactions include VAPA-BCAP31, BCAP31-LBR, LBR-TMPO, ATL3-SEC22B, and SEC22B-SEC23A.

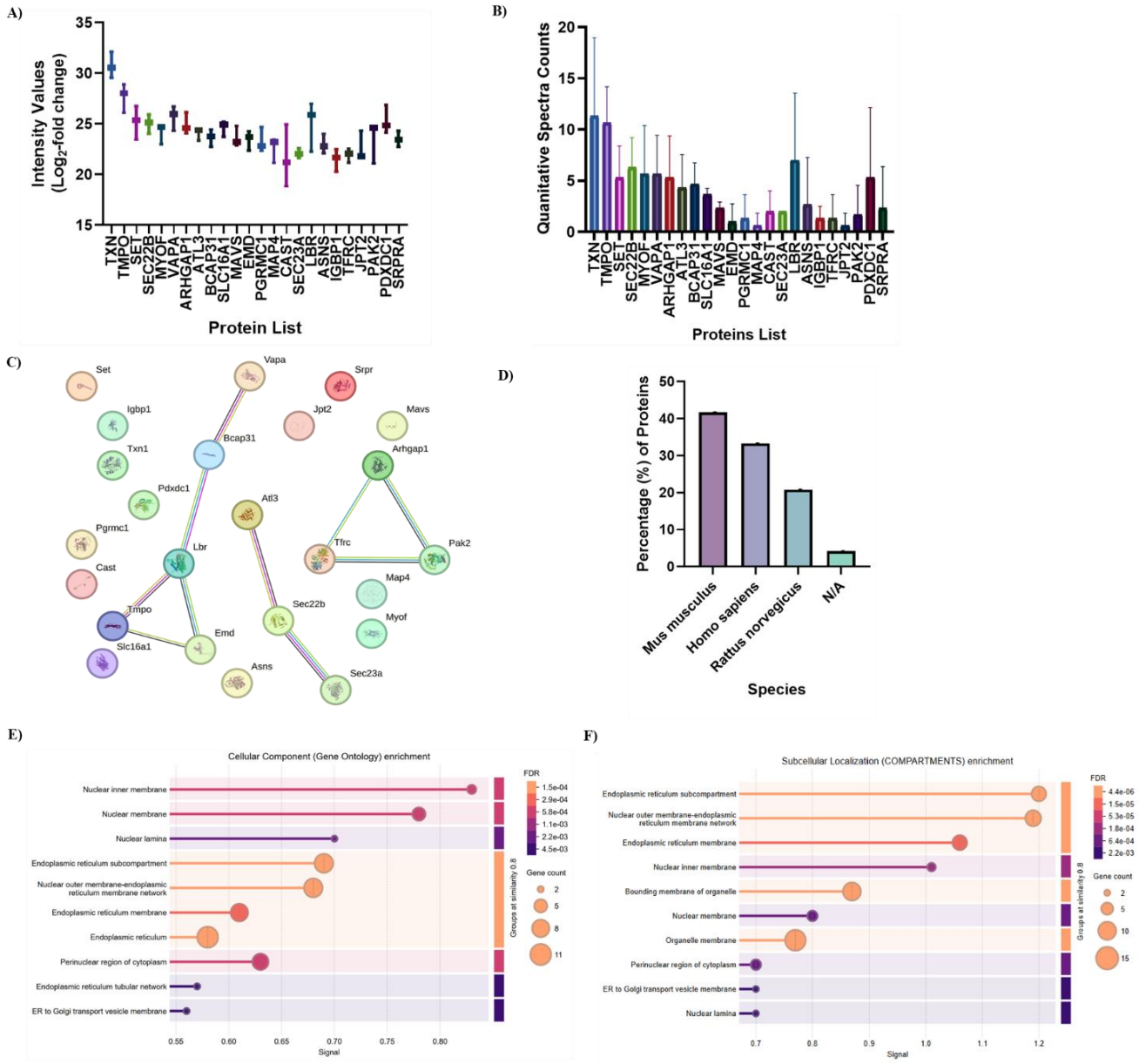

Figure 11. Characterization of LLC WT secreted proteins. A) Quantification of intensity values (log2-fold) of 24 secreted proteins, minimum number of peptides 2 and a 1.0% FDR cut-off (n=3). **B)** Quantitative average spectra counts of secreted proteins with a minimum peptide count of 2 and a 1.0% FDR cut-off, (n=3) **C)** STRING annotation revealing links between 24 proteins identified in all 3 trials after removal of contaminant/background proteins (n=3). **D)** Each of the 24 candidate proteins identified in our dataset was queried in Vesiclepedia to determine in which species' EVs it had been previously reported. Proteins found in multiple species were assigned to a single species based on the following prioritization: Mus musculus >

Homo sapiens > Rattus norvegicus > N/A. The bar graph displays the percentage of proteins assigned to each species, normalized to the total number of proteins. **E)** Cellular component enrichment graph of the 24 proteins (n=3). **F)** Subcellular localisation enrichment graph of the 24 proteins (n=3). Graphs **D)** and **E)** generated by STRING database.

Between the 3 trials, 24 unique proteins are derived from extracellular vesicles with 42% derived from musculus exosomes, 33% from homo sapiens exosomes, 21% from rattus norvegicus, and 4% not exosome related (Fig 11. D). This indicates that the majority of proteins found are secreted via extracellular vesicles (EVs) and/or are EV-related such as TFRC (Transferrin receptor protein 1) and VAPA (Vesicle-associated membrane protein-associated protein A). Additionally, a study comparing the secreted secretome of C26 and EL4 demonstrates the presence of SET, MYOF, ARHGAP1, ATL3, SLC16A1, ASNS, TFRC, and PAK2 in the cancer cell line small extracellular vesicle (sEV) cargo[65]. The presence of the following secreted proteins was also confirmed: TMPO, VAPA, CAST, and SEC23A[65].

On the other hand, thioredoxin (TXN), a protein that has been found to be secreted via a leaderless secretory pathway, is also detected[66]. TXN has the highest intensity and spectral counts recorded (Fig 11. A, B). TXN is overexpressed in many cancer types and has been found to contribute to tumour growth, immune evasion, angiogenesis, and drug resistance by protecting tumour cells from oxidative stress[66,67]. Furthermore, many of the proteins detected are likely involved in membrane-associated processes, particularly those related to the nuclear envelope, ER, and possibly protein trafficking (Fig 11. E, F). Their localization highlights roles in organelle interaction and intracellular transport, consistent with processes like protein folding, secretion, or organelle communication (Fig 11. E. F).

4.2.5. Secreted proteins linked to secretory pathways and distinct secretome between LLC WT and MC38 WT secretome.

Gene ontology analysis of the differentially expressed 24 secreted proteins was conducted (Figure 12. A, B)), and they were cross referenced with RNA sequencing data of LLC WT and MC38 WT adherent cell lines whole cell data (Fig 12. C). Similar to previous enrichment results the GO biological processes data reveals proteins predominantly involved with transportation indicating the secreted proteins are tightly linked to normal secretory pathways (Fig 12. A). The top terms included the nuclear membrane, Golgi membrane, nuclear envelope, and nuclear inner membrane, suggesting captured proteins are localized to subcellular compartments involved in trafficking and membrane organization (Fig 12. B). Additional enrichment was observed for components such as coated vesicles, outer membranes, and the endoplasmic reticulum tubular network, further supporting the selective labeling of proteins involved in intracellular transport and vesicle dynamics (Fig 12. B).

Furthermore, secreted proteins reveal differential expression between LLC WT data and MC38 WT (Fig 12. C). Proteins highly expressed by LLC WT are lowly expressed by MC38 WT and vice-versa (Fig 12. C). These results provide further insight into the differences observed in causing atrophy *in vitro* between LLC WT and MC38 WT experiments previously demonstrated (Figure 1. B, C).

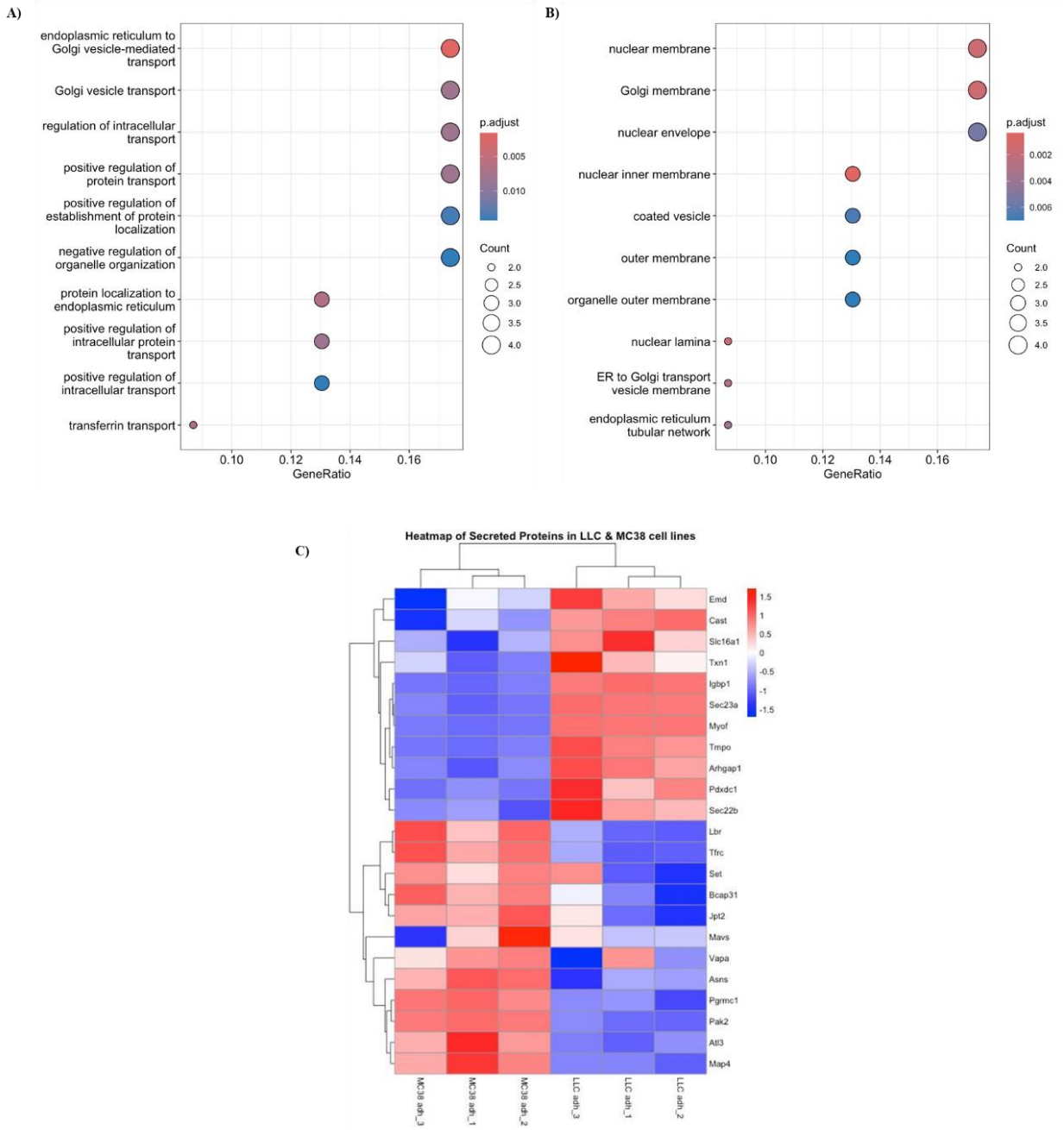

Figure 12. LLC WT secreted proteins gene ontology biological processes and cellular compartmentalization, and heatmap of RNA expression of secreted proteins in LLC WT and MC38 WT cells. A) Biological processes and **B)** cellular compartmentalization of the differentially expressed 24 secreted proteins derived from LLC WT cell lines stably expressing ER localized TurboID vector **C)** Secreted proteins cross-referenced with LLC WT RNA and MC38 WT RNA sequencing data. Red indicates high expression. Blue indicates low expression. Data presented as Log2 Fold Chain value (not p-adjusted). RNA data provided by A. Saleh (unpublished).

4.2.6. Secreted proteins downregulated and upregulated in C/EBPβ OE/KO RNA sequencing data

The 24 proteins were cross-referenced with RNA sequencing data from LLC KO (sg3) and OE (C/EBPβ) models (A. Saleh, unpublished) (Figure 13, A – F). RNA sequencing data looking at the 24 corresponding genes of the identified 24 proteins demonstrates that KO of C/EBPβ has a critical impact on the secretome when compared to OE of C/EBPβ based on the overall differential expression (Fig 13. A, B).

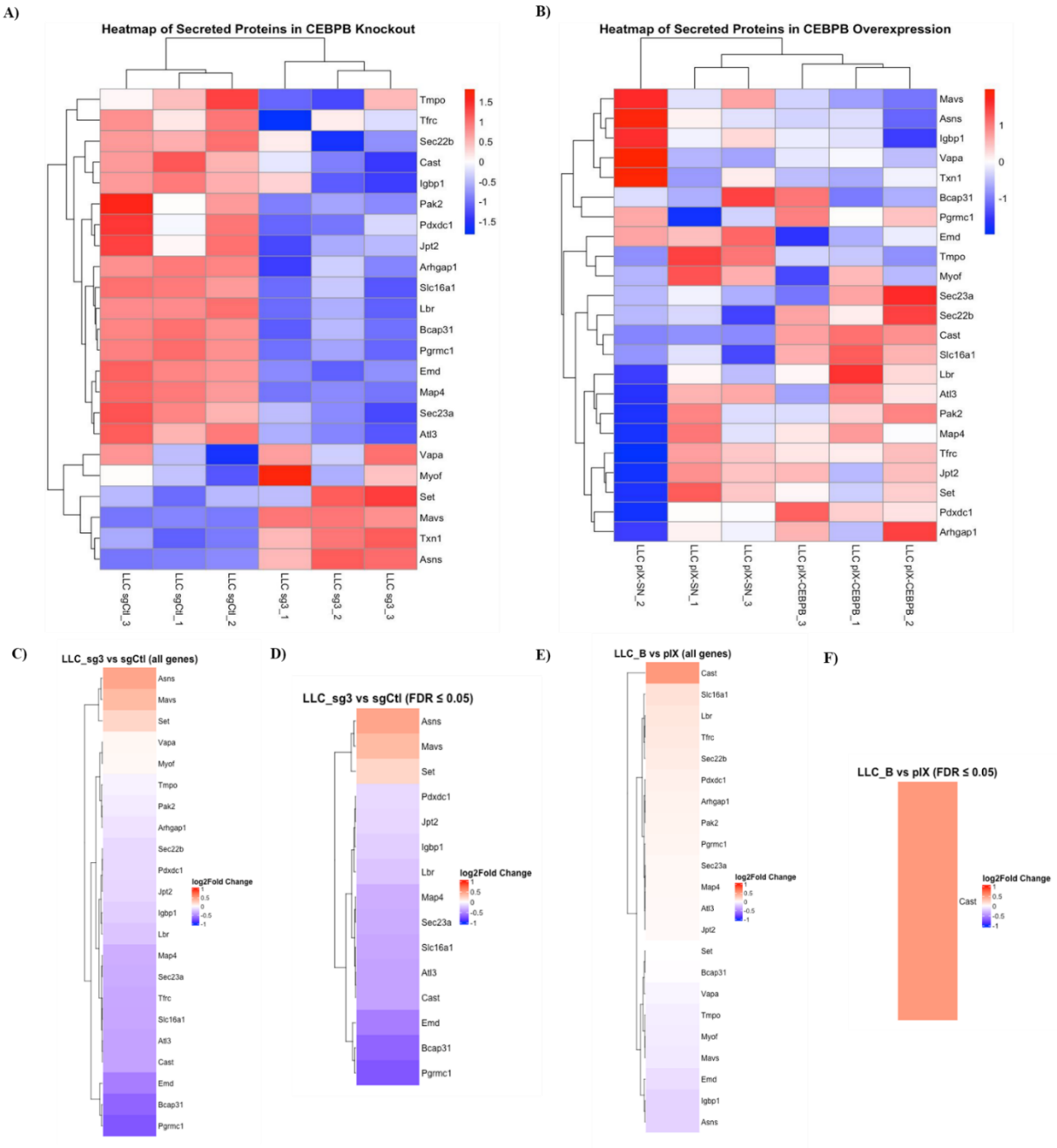

Figure 13. Heatmap of RNA expression of secreted proteins in LLC C/EBPβ Overexpression (OE) and Knockout (KO). A) 24 secreted proteins high and low expression in C/EBPβ KO (n=3). **B)** 24 secreted proteins high and low expression in C/EBPβ OE (n=3). **C)** Average of 3 trials for KO versus controls. **D)** Statistically significant up- or down-regulated genes for KO with an FDR ≤ 0.05 **E)** Average of 3 trials for OE versus controls. **F)** Statistically significant up-regulated gene, Cast, with an FDR ≤ 0.05. Red indicates high expression. Blue indicates low expression. Data presented as Log2 Fold Chain value (not p-adjusted, unless stated otherwise). RNA data provided by A. Saleh (unpublished).

The KO of C/EBPβ reveals several genes with low expression that have high expression in the control cell lines: *Cast, Pak2, Pdxdx1, Jpt2, Arhgap1, Slc16a1, Lbr, Bcap31, Pgrmc1, Emd, Map4, Sec23a, Atf3* (Fig 13 C). Whereas there are 3 genes that have high expression in the KO: *Mavs, Txn1, Asns* (Fig 13. C). These results indicate that KO of C/EBPβ appears to be critical in changing the secretome. Additionally, there are 13 genes that are statistically significant in the KO, in particular *Pgmc1, Bcap31, Emd*, and *Cast* are significantly downregulated (Fig. 13 C).

Whereas *Cast, Slc16a1*, and *Lbr* were among the few proteins that showed relatively high expression in the CEBPB OE condition while being downregulated in the KO condition (Fig 13. B). *Monocarboxylate transporter 1 (Slc16a1)* is a lactate transporter that is used to fuel tumour metabolism which has been associated with poor prognosis, metastasis, and larger tumour sizes[68]. *Delta(14)-sterol reductase LBR (Lbr)* is involved in cholesterol biosynthesis in which case could contribute to lipid-driven inflammation inducing cachexia[69,70]. However, when the trials are averaged and a false discovery rate (FDR) of less than or equal to 0.05 is applied to the OE genes, the only gene statistically upregulated is *Cast* (Fig 13. E, F). *Calpastatin (Cast)* has been demonstrated to regulate calpain, a protease that is implicated in muscle protein degradation[71].

5. DISCUSSION OF RESULTS

5.1 Summary of Key Findings

In this study, we investigated the role of CCAAT/Enhancer-Binding Protein *Beta* (C/EBPβ) in regulating the tumour-derived secretome responsible for cancer cachexia. Through conditioned media (CM) experiments, we observed that cancer cell lines with elevated C/EBPβ expression, such as LLC, were more likely to promote myotube atrophy, whereas those with lower expression levels, like EL4, exhibit minimal or no atrophic effects. This suggests a potential link between C/EBPβ expression and the capacity of tumor-secreted factors to induce muscle atrophy. Extracellular vesicles (EVs) and apoptotic bodies derived from LLC cell lines were shown to contribute significantly to myotube atrophy *in vitro*.

To further define the cancer cell-derived secretome, a TurboID-based proximity biotinylation system was developed and successfully integrated into multiple murine cancer cell lines, enabling the specific capture of secreted proteins from a cachexic model for mass spectrometry analysis. Through this approach, 24 secreted proteins were identified, many linked to vesicular pathways, and cross-referenced RNA-sequencing data revealed that C/EBPβ knockout (KO) exerts a greater impact on secretome composition than the overexpression (OE) of C/EBPβ in LLC cells. This was expected given that LLC cells already express C/EBPβ, and knockdown down of C/EBPβ restores myotube diameter and differentiation *in vitro* and prevents muscle wasting *in vivo*[3]. Whereas OE of C/EBPβ is non-cachectic tumours like EL4 converted a non-cachectic secretome into a cachectic one [3]. Overall, these findings highlight C/EBPβ as a central regulator of cachexia-inducing secreted factors and demonstrate the utility of TurboID in secretome profiling.

5.1.1 C/EBPβ expression correlates with atrophy in a cell specific manner

The results presented in Figure 1 illustrate that the expression of C/EBPβ correlates with atrophy in a cell specific manner. Cancer cell lines LLC and MC38 express C/EBPβ, however have different *in vitro* phenotypes regarding atrophy. While MC38 was found to be non-atrophic *in vitro*, it is highly cachectic *in vivo* (N. Strong, unpublished). The difference between LLC and MC38 opposite atrophy-inducing *in vitro* phenotypes may have to do with their respective secretomes. For example, signalling pathways disrupted in LLC include PI3K/AKT/mTOR[72], RTK/RAS[73], p53[73], TGFβ[73], and Hippo[73]. In contrast, MC38 exhibits alterations in pathways such as EGFR, WNT/β-catenin, TGF-β, and downstream MAPK[74,75]. LLC tumours were also characterized as poorly immunogenic[76], while MC38 tumours are characterized as moderately immunogenic[77,78]. Although TGF-β signaling is disrupted in both tumor models, the broader differences in affected pathways likely contribute to distinct secretome profiles between LLC and MC38. Moreover, while LLC tumours are consistently demonstrated to be cachectic *in vitro* and *in vivo*[3,79], MC38 has been described as both non-cachectic and cachectic *in vitro* and *in vivo*[80–82].

Studies have demonstrated that blocking of a single cachexic factor does not prevent the progression of cachexia, and rather cancer cachexia factors tend to work in collaboration via different interactions[15]. Additionally, there is cross-communication between different organs (i.e brain, pancreas, heart, spleen, etc) with skeletal muscle in cancer cachexia by complex signal exchanges between organs[15]. This cross communication includes brain to muscle, bone to muscle, and gut microbiota to muscle and adipose which contribute to the catabolism of tissue and has been implicated in a tumour macroenvironment[83]. For this reason, LLC may have a direct mechanism in inducing cachexia both *in vitro* and *in vivo*, whereas MC38 may rely on a

distinct cell population to drive cachexia indirectly via the use of crosstalk between different organs and/or collaboration between different secreted factors[15,83].

Moreover, a study demonstrates that in LLCs, cachexia can be induced through a direct signaling mechanism targeting skeletal muscle, independent of host-derived secreted factors[84]. This is done through the activation of p38β MAPK in skeletal muscle, which in turn phosphorylates C/EBPβ increasing its ability to bind DNA and activate the promoter of the atrogin1/MAFbx gene[84]. This results in increased expression of atrogin1/MAFbx, a key E3 ubiquitin ligase in the ubiquitin-proteasome system (UPP), leading to muscle protein breakdown and atrophy independent of host derived factors and systemic inflammation[84]. Whereas MC38 may rely on cross-communication between different organs (i.e. with the brain, bone, microbiota) and host derived factors[83].

Given that MC38 is a colon cancer, another type of colon cancer known as C-26 has demonstrated significant microbiome composition changes which correlated with cachexic phenotypes[83]. Moreover, one study demonstrates that significantly altering the microbiota of mice, results in the inhibition of MC38 tumour growth by interfering with amino acid and lipid metabolism[85]. For this reason, cross communication between MC38 and changes of the gut microbiota may be one of the mechanisms of inducing cachexia *in vivo*.

Furthermore, each cell line has its own level of C/EBPβ and its expression is sufficient in inducing atrophy, as seen for LLC, MC38 (*in vivo*), B16, and GL261. Given B16 induces significant atrophy *in vitro*, suggests it's secretome may secrete various cachexia-inducing factors (CIFs). Although a related variant, B16-F10, has been demonstrated to be cachectic *in vivo*[86], B16 itself has not been assessed *in vivo* and therefore *in vivo* studies should follow. GL261, by contrast, has been demonstrated to be cachectic *in vivo*[87]. Given that KO of C/EBPβ

in cachectic cell line, LLC, resulted in a non-cachectic one[3], loss of function (LOF) of C/EBPβ should be conducted for B16, MC38, and GL261 to assess the impact of loss of C/EBPβ on these potentially cachectic secretomes.

Conversely, cell lines that do not express C/EBPβ such as CT2A, ID8, and EL4 are non-atrophic *in vitro*. ID8 was found to produce small primary tumours[88], however it has not been established as a cachectic or non-cachectic cancer cell line yet. Similarly, CT2A has not been established as a cachectic or non-cachectic model. Moreover, when non-cachectic cancer cell line, EL4, was OE with C/EBPβ, the secretome converted to a cachexic one[3], for this reason gain of function (GOF) studies should be conducted for CT2A, ID8, and EL4.

In parallel, assessing C/EBPβ activity across all seven murine cancer cell lines will provide valuable insight into its functional dynamics and potential contribution to tumor-driven cachexia. This is important given that C/EBPβs ability to bind DNA is not dependent on its expression level but rather on its phosphorylation state[84]. C/EBPβ activity is regulated by several protein kinases and the sites it is phosphorylated, which influence its activity, cellular location, and whether it is gene activating or repressing[89,90]. In general, a transcription factor's activity can be repressed[91] by transcriptional repression (i.e. siRNA[92], Crisper interference[93]), post translational modifications (i.e C/EBPβ transactivation can be inhibited by insulin via the PI 3-kinase pathway[89]), and blocking nuclear localization[94] (i.e trapping C/EBPβ in the cytoplasm) to prevent access to DNA. Moreover, C/EBPβ is also a druggable target and can be inhibited by a natural compound (Withaferin A)[95], selective peptide antagonist (ST101)[96], and a synthetic analog (helenalin mimic)[97]. By decreasing and/or inhibiting C/EBPβ activity in cancer cell lines it is expected that genes that are transactivated would decrease and/or be inhibited resulting in a non-cachectic secretome and/or decrease in myotube atrophy. The drugs mentioned above all

exhibit anti-tumour activities[95–97], and thereby demonstrate that the inhibition of C/EBPβ as a potential therapeutic strategy in the context of cancer cachexia[3,95].

5.1.2 Atrophy-inducing and non-atrophic cancer cell lines release similar concentrations of EVs but differ in their EV size distributions

EVs refer to all membrane bound vesicles that are secreted into the extracellular space which include exosomes, microvesicles (MVs), and apoptotic bodies[30]. Nanoparticle tracking analysis (NTA) was used to assess the overall concentrations and size distributions of EVs across seven murine cancer cell lines. While the EV concentrations normalized to protein content were not significantly different across the cell lines, differences in EV median size were observed (Figure 2A, B). As part of our first aim, these results indicate that EV concentration is independent of whether the cancer cell lines are categorized as atrophy-inducing or non-atrophic. However, EV median size varied depending on the cancer cell line. Notably, non-atrophic models (EL4, ID8, and MC38) produced relatively larger EVs compared to the atrophic model (B16) (Figure 1. C). LLCs derived EVs on the other hand are not statistically different from either group (Fig 2. B).

Our findings do not show a consistent relationship between C/EBPβ LAP isoform expression and EV concentration or size across the cancer cell lines tested. While MC38 and LLC cells exhibited relatively higher LAP expression and variable EV levels, other lines such as ID8 and CT2A produced comparable or greater numbers of EVs despite low LAP expression. This suggests that C/EBPβ may not be a universal regulator of EV biogenesis in cancer cells, or that its effects are context-dependent and influenced by additional factors such as cell type. Further studies using C/EBPβ KO or OE models are needed to dissect its specific role in EV production.

Given that EV cargo is cell-type specific and that the overall content of EVs is reflective of the cell of origin[98], these differences in size may indicate the overall composition of the EV cargo. For example, a study examining cardiac progenitor cell (CPC)-derived sEVs found that there are functional differences in the subpopulations of sEVs, where small and medium sized sEVs demonstrated effects on functional assays whereas large sized sEVs had no effect[99]. For this reason, it could be that smaller EVs may have functional differences when compared to the larger EVs which are found in non-atrophic models.

A limitation of this analysis is that exosomes and microvesicles were not separated prior to measurement which may influence the average sizes described. Thus, the reported EV concentrations and sizes represent a mixed population. Given the differences in size and biogenesis between exosomes and microvesicles, future studies should aim to separately characterize these EV subtypes to better understand their potential contributions to cachexia.

5.1.3 LLC derived extracellular vesicles, and apoptotic bodies contribute to wasting in vitro

EVs have been implicated in a variety of cancer types in regard to influencing the progression and metastasis of cancer and modulating the tumour microenvironment[100]. Given the role of EVs in cancer, researchers are looking into the emerging role of EVs in cancer cachexia[101]. We conducted conditioned medium (CM) experiments looking at EVs and apoptotic bodies and their effects on myotube atrophy *in vitro*. The apoptotic body CM experiment examined the role of apoptotic bodies derived from LLC and whether they would induce myotube atrophy, whereas the EV-CM experiments were exploring the role of exosomes and microvesicles derived from LLC, MC38, and EL4 wild-type cancer cell lines.

Apoptotic bodies and EVs derived from LLC contribute to atrophy as seen by a decrease in myotube diameter. When CM was completely depleted of all EVs (exosomes, microvesicles (MVs), and apoptotic bodies), there was no change in myotube diameter, indicating the significant role that EVs derived from LLC have in cancer cachexia. This indicates that the removal of all EVs results in a protective effect. Moreover, a limitation to this study is that EVs were not purified further after ultracentrifugation steps in which case the effects observed may also be due to co-precipitated proteins present that are attached to the EVs. Furthermore, as discussed above given that the type of EV and size of EVs can have different effects, the experiment should be conducted again with only removal of each subtype of EV (i.e exosomes, MVs) to determine whether one drives the atrophic phenotype more strongly than others.

However, the treatment with apoptotic bodies and apoptotic body-free conditioned medium CM (apo-free CM) does not induce the same level of wasting or protective effect as compared to C2C12s treated with only EVs (exosomes and MVs) or EV-free CM. For reference, the apo-free CM is devoid of apoptotic bodies but still contains extracellular vesicles (EVs), including exosomes and MVs. This suggests that the combined presence of all three EV subtypes may be necessary to fully induce cachexia, as each subtype likely carries distinct cargo[102] that contributes to the multifactorial nature of the wasting response[103].

5.1.4 EVs derived from non-atrophic cell lines do not contribute to wasting in vitro

In contrast, EVs derived from non-atrophic cancer cell lines, MC38 and EL4, have no effect on myotube diameter. While no EV-mediated effects can be observed *in vitro*, this may not fully recapitulate the systemic crosstalk that occurs *in vivo*. The possibility that tumor-derived EVs interact with other organs to generate a cachexia-inducing secretome underscores the need for *in vivo* validation. Thereby, *in vivo* experiments should be followed with MC38 WT derived

EVs (given that MC38 has been shown to be cachexic *in vivo*, N. Strong, unpublished) to determine whether they facilitate communication between the tumor and skeletal muscle and modulate the tumor microenvironment in the context of cancer cachexia.

5.1.5 TurboID machinery successfully labels intracellular proteins and biotin tags allow for the successful capture of secreted proteins

As part of Aim 2, the overarching goal was to develop a TurboID based system to label and identify secreted proteins and assess a C/EBPβ regulated secretome. To facilitate this TurboID was successfully expressed as observed by the presence of the anti-V5 tag in 7 cancer cell line constructs which included wildtype, gain of function (GOF) of C/EBPβ, and loss of function (LOF) of C/EBPβ models. Additionally, the activity of the TurboID enzyme was confirmed as cell lines exposed to exogenous biotin revealed the presence of biotin tagged proteins via immunoblotting of Streptavidin-HRP, when compared to controls which did not detect tagged proteins in the absence of exogenous biotin. Additionally, the data presented illustrates that longer incubation of the cancer cell lines leads to more proteins tagged with biotin intracellularly (Figure 7). However, a limitation of prolonged biotin incubation is the increased background labeling resulting from the high activity of TurboID[104]. This can lead to the biotinylation of distal or non-specific proteins, which may pose a challenge for future experiments aiming to identify specific protein-protein interactions[4].

All 7 seven cell lines expressing the TurboID vector were grown in the presence or absence of exogenous biotin and conditioned media was collected after to assess whether proteins tagged with biotin were secreted by the cell lines. Our data reveals that proteins tagged with biotin were successfully secreted and captured via the use of streptavidin coated beads (Figure 8. D, E). However, in CM derived from controls (i.e no exogenous biotin added), there is

high background seen. This background can be attributed to streptavidin from the streptavidin coated magnetic beads which have a molecular weight of 76 kDa.

5.1.6 LLC WT secretome reveals capture of 24 proteins

Using the TurboID technology we were able to identify 24 proteins secreted across the 3 replicates (Trial 1, 2, and 3). However, Trial 1 had a much higher yield of identified proteins when compared to Trial 2 and 3. On further inspection, it was found that Trial 1 and controls contained several nuclear, pro-apoptotic, and housekeeping proteins indicative of elevated levels of cell lysis, and thereby a capture of significantly more proteins. Another factor that may contribute to the decreased number of proteins identified may have to do with the activity of the TurboID enzyme[104]. TurboID has been demonstrated to cause cellular toxicity due to its high activity and biotin affinity[64]. A study investigating constitutive TurboID expression in Drosophila tissues reported reduced survival rates and smaller body sizes, attributed to excessive biotin depletion in the absence of biotin supplementation[4]. Whereas prolonged activation of TurboID can lead to growth defects due to over biotinylation of the proteome[4,64]. For this reason, trials 2 and 3 may have had fewer proteins identified due to cellular growth defects and compromised cellular integrity associated with high TurboID activity, which could have impaired protein processing, secretion, or recovery. Overall, the differences in proteins observed in trial 1 and trial 2 and 3, indicate that more replicates in the future should be conducted to account for differences in MS data[105].

The identification of 24 secreted proteins from a cachexic model still provides a valuable foundation for confirming the use of a TurboID approach to study the secretome, and insight into factors that may contribute to its cachexic secretome. Many of the proteins identified are found as extracellular vesicle cargo derived from a variety of species. In particular, the highest detected

protein is TXN (thioredoxin) which is also known to be secreted[66], followed by TMPO (Thymopoietin), and LBR (Delta(14)-sterol reductase LBR). TXN is found to be elevated in many human cancers, where its overexpression is associated with inhibition of apoptosis, aggressive tumour growth, resistance to anti-cancer therapies, and reduced patient survival[106]. TXN can also enhance the DNA-binding activity of nuclear NF-κB[107], thereby amplifying pro-inflammatory signaling by NF-κB which has been implicated in cancer cachexia[108]. Additionally, TMPO has been demonstrated to be upregulated in a variety of cancer types and leads to poor prognosis in patients[109]. Given that all of these proteins are secreted, they may contribute to muscle wasting by triggering an immune response in C2C12 myotubes, promoting local inflammation and activating proteolytic pathways.

Whereas, LBR has been found to be apart of the cholesterol biosynthesis metabolic pathway[110,111]. Tumour cells require high amounts of cholesterol to maintain cell proliferation, and thereby tumorigenesis is often associated with dysregulated cholesterol biosynthesis[112]. Additionally, secreted LBR may disrupt cholesterol balance within muscle cells, triggering membrane stress, ER dysfunction, or inflammatory signaling pathways. Notably, that activation of endoplasmic reticulum (ER) stress-induced unfolded protein response (UPR) has been implicated in cancer-induced muscle wasting[113]. Together, these insights suggest the notion that cholesterol dysregulation may be a contributor to muscle wasting in cachexia.

Other proteins identified in our MS data such as myoferlin (MyoF) and asparagine synthetase (ASNS), have also been implicated in cancer progression and metastasis[114,115]. Myoferlin (MyoF), which showed relatively high intensity in our dataset, is known to be overexpressed in various cancers and promotes cancer cell invasion and migration[114]. Interestingly, in breast and pancreatic cancer models, MyoF has been identified as a regulator of

exosome composition and function[114]. While its loss does not prevent exosome formation, it alters exosomal cargo, reduces uptake by recipient cells, and impairs tumor supportive processes such as angiogenesis[114]. These findings raise the possibility that MyoF may similarly contribute to exosome uptake and signaling in other cancer types, including LLC, though this remains to be experimentally validated. Furthermore, ASNS has been shown to modulate skeletal muscle satellite cells (SMSCs) by promoting proliferation and inhibiting differentiation[116]. Given that impaired SMSC differentiation is a feature of muscle-wasting conditions such as cachexia[117], these findings raise the possibility that ASNS may contribute to such muscle wasting, however this remains to be directly tested.

Moreover, functional annotation and STRING network analyses revealed that nearly half of the 24 proteins identified are associated with exosomes, supporting the idea that extracellular vesicles are central to tumour and host communication in cachexia. Furthermore, many of the proteins identified such as TXN, VAPA, ASNS, and CAST, are involved in stress responses, metabolism, and intracellular trafficking. These findings align with known features of the cachexia-inducing secretome.

Since nearly half of the identified proteins are found as EV cargo, further investigation into the protein cargo (i.e RNA, DNA, protein, etc.) of these vesicles could provide deeper insights into the cachexia-inducing phenotype of LLC cells, which could then be compared to GOF/LOF C/EBPβ models to provide further understanding of the role of C/EBPβ in modulating the cachectic secretome.

5.1.7 Knockout of C/EBPβ is critical in modulating the LLC secretome

Cross-referencing these proteins with RNA-sequencing data from C/EBPβ overexpression and knockout models further supports this regulatory role. Several genes,

including *Set, Asns,* and *Mavs*, were downregulated in C/EBPβ OE models, while others like *Cast, Slc16a1*, and *Lbr* were upregulated, suggesting that C/EBPβ exerts both positive and negative transcriptional control over specific secretome components[23]. In particular, the KO model significantly downregulates *Pgmc1, Bcap31, Emd*, and *Cast*, whereas the OE model significantly upregulates *Cast (calpastatin)*. A proteolytic system involving *Cast* has been found to inhibit *Calpain* which causes muscle breakdown[118,119]. Interestingly, a study overexpressing *Cast* did not prevent muscle atrophy indicating that the targetting of one proteolytic system is not effective, and a more integrated approach is needed[118].

Overall, these findings provide evidence that C/EBPβ regulates a distinct subset of secreted proteins capable of contributing to the cachectic phenotype. The use of TurboID enabled the specific isolation of these proteins, aiding in overcoming technical challenges in traditional secretome profiling. These results not only validate C/EBPβ as a central regulator of the tumour secretome but also establish a framework for future *in vivo* studies using stable TurboID expressing cell lines to map systemic protein trafficking and its impact on host tissues and/or organs.

5.1.8 Future use of TurboID for in vivo proteomic mapping and understanding of communication networks

In future studies, the stable creation of these cancer cell lines stably expressing TurboID can be used in animal models to analyze *in vivo* proteomic mapping[120], where mouse models will be inoculated with tumour cell lines expressing the promiscuous biotin ligase[43]. This will allow for the mapping of cancer secreted factors as they will be distinguished from the host's secreted factors by in vivo biotinylation to reveal the uptake of the secreted factors in distal organs[43]. This *in vivo* proteomic mapping will determine whether cancer-secreted proteins and EVs reach

skeletal muscle and other organs, shedding light on the mechanisms contributing to the observed promotion of myotube atrophy in cancer cachexia.

A possible limitation of this model is the potential discrepancies between secreted factors identified *in vitro*, which may not reflect whole tumour secretomes *in vivo*[121]. Indeed, tumours in vivo include multiple cell types beyond the malignant cells including immune cells and cancer-associated fibroblasts. Thus, the tumour cell secretome identified in culture is likely only a part of the tumour secretome *in vivo*[122–124]. Additionally, inoculation of cancer cell lines at different anatomical locations may result in different secretome compositions due to the differences in tumour microenvironment (TME) which are tissue-specific[125]. To address this, all tumours should be inoculated in consistent ways and the same muscle types/organs should be initially harvested for MS as described in established methods[126]. Following this, other tissue types/organs should be harvested and an analysis comparing each anatomical location's secretome should be compared. This will provide insight into the differences of secretome across tissue types and the different mechanisms the tumours may employ in driving cachexia.

6. CONCLUSION

While significant progress has been made in understanding the molecular mechanisms underlying cancer cachexia[127], much work remains to be done to translate these findings into effective therapies for patients[128]. Continued research efforts aimed at unraveling the complexities of the cachexia-inducing secretome[17] and identifying novel therapeutic targets are essential for improving outcomes and quality of life for cancer patients[17]. This research advances this field by providing more insight into the role of C/EBPβ in the development of cancer cachexia[3] and allows for the mapping of protein communication both *in vitro* and with future studies, *in vivo*. Currently, there is no cure for cancer cachexia, and cachexia patients also have significant morbidity and poor tolerance to chemotherapy[1,3].

Overall, this study highlights the critical role of C/EBPβ in regulating the tumour-derived secretome associated with cancer cachexia. Using a combination of conditioned media experiments and extracellular vesicle isolation, we demonstrated that cancer cell lines with elevated C/EBPβ expression, such as LLC, induce significant myotube atrophy *in vitro*, and that LLC-derived extracellular vesicles and apoptotic bodies are major contributors to this atrophic phenotype. In contrast, EVs derived from non-atrophic models, such as MC38 and EL4, did not induce myotube atrophy *in vitro*, suggesting distinct secretome signatures between atrophy-inducing and non-atrophic cancer types.

To further dissect the secreted factors responsible for these effects, we developed a TurboID-based biotinylation system for secretome profiling. This approach enabled the successful capture and identification of secreted proteins under physiologically relevant conditions. Mass spectrometry analysis revealed 24 unique proteins enriched in the cachectic secretome, many of which are associated with vesicular transport and stress response pathways.

Cross-referencing with RNA-sequencing data confirmed that knockout of C/EBPβ had a more profound effect on secreted gene expression profiles than overexpression, further emphasizing the central role of C/EBPβ in maintaining the cachectic secretome.

These findings emphasize the importance of C/EBPβ in the regulation of tumour-derived factors that drive cancer cachexia and demonstrate the utility of TurboID proximity biotinylation for high specificity secretome profiling. Future work expanding on these findings could promote the development of therapeutic strategies aimed at targeting cachexia-inducing secreted factors or extracellular vesicle cargo in cancer patients.

7. BIBLIOGRAPHY

1. Aoyagi, T., Terracina, K. P., Raza, A., Matsubara, H. & Takabe, K. Cancer cachexia, mechanism and treatment. *World J Gastrointest Oncol* **7**, 17 (2015).
2. Ottery, F. D. Cancer cachexia: prevention, early diagnosis, and management. *Cancer Pract* **2**, 123–31 (1994).
3. AlSudais, H., Rajgara, R., Saleh, A. & Wiper-Bergeron, N. C/EBPβ promotes the expression of atrophy-inducing factors by tumours and is a central regulator of cancer cachexia. *J Cachexia Sarcopenia Muscle* **13**, 743–757 (2022).
4. Branon, T. C. *et al.* Efficient proximity labeling in living cells and organisms with TurboID. *Nat Biotechnol* **36**, 880–887 (2018).
5. Kim, S. K. & Cho, S. W. The Evasion Mechanisms of Cancer Immunity and Drug Intervention in the Tumor Microenvironment. *Front Pharmacol* **13**, (2022).
6. Cooper, G. M. The Development and Causes of Cancer. in *The Cell: A Molecular Approach* (Sinauer Associates, 2000).
7. Government of Canada. Release notice - Canadian Cancer Statistics 2021. *Health Promotion and Chronic Disease Prevention in Canada* **41**, 399–399 (2021).
8. Canadian Cancer Society. Cancer statistics at a glance. *Canadian Cancer Statistics* (2023).
9. Lim, S., Brown, J. L., Washington, T. A. & Greene, N. P. Development and progression of cancer cachexia: Perspectives from bench to bedside. *Sports Medicine and Health Science* **2**, 177–185 (2020).
10. Liu, Y., Saavedra, P. & Perrimon, N. Cancer cachexia: lessons from *Drosophila*. *Dis Model Mech* **15**, (2022).
11. Poulia, K. A. *et al.* Pancreatic Cancer and Cachexia—Metabolic Mechanisms and Novel Insights. *Nutrients* **12**, 1543 (2020).
12. Zhu, R. *et al.* Updates on the pathogenesis of advanced lung cancer-induced cachexia. *Thorac Cancer* **10**, 8–16 (2019).
13. Liu, N., Li, S., Jia, J., Qiao, Y. & Li, Y. Advanced breast cancer with cachexia. *Medicine* **100**, e24397 (2021).
14. Ni, J. & Zhang, L. Cancer Cachexia: Definition, Staging, and Emerging Treatments . *Cancer Manag Res* **Volume 12**, 5597–5605 (2020).
15. Wang, Y., Dong, Z., An, Z. & Jin, W. Cancer cachexia: Focus on cachexia factors and inter-organ communication. *Chin Med J (Engl)* **137**, 44–62 (2024).
16. Donohoe, C. L., Ryan, A. M. & Reynolds, J. V. Cancer Cachexia: Mechanisms and Clinical Implications. *Gastroenterol Res Pract* **2011**, 1–13 (2011).

17. Freire, P. P. *et al.* The expression landscape of cachexia-inducing factors in human cancers. *J Cachexia Sarcopenia Muscle* **11**, 947–961 (2020).

18. Loumaye, A. & Thissen, J.-P. Biomarkers of cancer cachexia. *Clin Biochem* **50**, 1281–1288 (2017).

19. Prado, B. L. & Qian, Y. Anti-cytokines in the treatment of cancer cachexia. *Ann Palliat Med* **8**, 67–79 (2019).

20. Jiang, Z., Clemens, P. R., Jiang, Z. & Clemens, P. R. Cellular caspase-8-like inhibitory protein (cFLIP) prevents inhibition of muscle cell differentiation induced by cancer cells. *The FASEB Journal* **20**, 2570–2572 (2006).

21. Vishnoi, K., Viswakarma, N., Rana, A. & Rana, B. Transcription Factors in Cancer Development and Therapy. *Cancers (Basel)* **12**, (2020).

22. Bushweller, J. H. Targeting transcription factors in cancer — from undruggable to reality. *Nat Rev Cancer* **19**, 611–624 (2019).

23. Tolomeo, M. & Grimaudo, S. The 'Janus' Role of C/EBPs Family Members in Cancer Progression. *Int J Mol Sci* **21**, (2020).

24. De Felice, F. & Ferreira, S. Novel neuroprotective, neuritogenic and anti-amyloidogenic properties of 2,4-dinitrophenol: The gentle face of Janus. *IUBMB Life (International Union of Biochemistry and Molecular Biology: Life)* **58**, 185–191 (2006).

25. Ramji, D. P. & Foka, P. CCAAT/enhancer-binding proteins: structure, function and regulation. *Biochem J* **365**, 561–75 (2002).

26. Klijn, C. *et al.* A comprehensive transcriptional portrait of human cancer cell lines. *Nat Biotechnol* **33**, 306–312 (2015).

27. Matherne, M. G., Phillips, E. S., Embrey, S. J., Burke, C. M. & Machado, H. L. Emerging functions of C/EBPβ in breast cancer. *Front Oncol* **13**, (2023).

28. Okazaki, K. *et al.* CEBPB is required for NRF2-mediated drug resistance in NRF2-activated non-small cell lung cancer cells. *The Journal of Biochemistry* **171**, 567–578 (2022).

29. Ritchie, S., Reed, D. A., Pereira, B. A. & Timpson, P. The cancer cell secretome drives cooperative manipulation of the tumour microenvironment to accelerate tumourigenesis. *Fac Rev* **10**, 4 (2021).

30. Doyle, L. M. & Wang, M. Z. Overview of Extracellular Vesicles, Their Origin, Composition, Purpose, and Methods for Exosome Isolation and Analysis. *Cells* **8**, (2019).

31. van Niel, G., D'Angelo, G. & Raposo, G. Shedding light on the cell biology of extracellular vesicles. *Nat Rev Mol Cell Biol* **19**, 213–228 (2018).

32. Chitti, S. V., Fonseka, P. & Mathivanan, S. Emerging role of extracellular vesicles in mediating cancer cachexia. *Biochem Soc Trans* **46**, 1129–1136 (2018).

33. Marzan, A. L. & Chitti, S. V. Unravelling the Role of Cancer Cell-Derived Extracellular Vesicles in Muscle Atrophy, Lipolysis, and Cancer-Associated Cachexia. *Cells* **12**, 2598 (2023).

34. Hu, W. *et al.* Lung cancer-derived extracellular vesicles induced myotube atrophy and adipocyte lipolysis via the extracellular IL-6-mediated STAT3 pathway. *Biochimica et Biophysica Acta (BBA) - Molecular and Cell Biology of Lipids* **1864**, 1091–1102 (2019).

35. Pin, F. *et al.* Extracellular vesicles derived from tumour cells as a trigger of energy crisis in the skeletal muscle. *J Cachexia Sarcopenia Muscle* **13**, 481–494 (2022).

36. Chitti, S. V. *et al.* Proteomic analysis of the small extracellular vesicles and soluble secretory proteins from cachexia inducing and non-inducing cancer cells. *Proteomics* **23**, (2023).

37. Massart, I. S. *et al.* Marked Increased Production of Acute Phase Reactants by Skeletal Muscle during Cancer Cachexia. *Cancers (Basel)* **12**, 3221 (2020).

38. Anand, S., Samuel, M., Ang, C.-S., Keerthikumar, S. & Mathivanan, S. Label-Based and Label-Free Strategies for Protein Quantitation. in 31–43 (2017). doi:10.1007/978-1-4939-6740-7_4.

39. Li, Z. *et al.* Systematic Comparison of Label-Free, Metabolic Labeling, and Isobaric Chemical Labeling for Quantitative Proteomics on LTQ Orbitrap Velos. *J Proteome Res* **11**, 1582–1590 (2012).

40. O'Connell, J. D., Paulo, J. A., O'Brien, J. J. & Gygi, S. P. Proteome-Wide Evaluation of Two Common Protein Quantification Methods. *J Proteome Res* **17**, 1934–1942 (2018).

41. Dowell, J. A., Wright, L. J., Armstrong, E. A. & Denu, J. M. Benchmarking Quantitative Performance in Label-Free Proteomics. *ACS Omega* **6**, 2494–2504 (2021).

42. Schiapparelli, L. M. *et al.* Direct Detection of Biotinylated Proteins by Mass Spectrometry. *J Proteome Res* **13**, 3966–3978 (2014).

43. Droujinine, I. A. *et al.* Proteomics of protein trafficking by in vivo tissue-specific labeling. *Nat Commun* **12**, 2382 (2021).

44. Wei, W. *et al.* Cell type-selective secretome profiling in vivo. *Nat Chem Biol* **17**, 326–334 (2021).

45. Niinae, T., Ishihama, Y. & Imami, K. Biotinylation-based proximity labelling proteomics: basics, applications and technical considerations. *The Journal of Biochemistry* **170**, 569–576 (2021).

46. Cvjetkovic, A. *et al.* Detailed Analysis of Protein Topology of Extracellular Vesicles–Evidence of Unconventional Membrane Protein Orientation. *Sci Rep* **6**, 36338 (2016).

47. Méndez, O. & Villanueva, J. Challenges and opportunities for cell line secretomes in cancer proteomics. *Proteomics Clin Appl* **9**, 348–357 (2015).

48. Xue, H., Lu, B. & Lai, M. The cancer secretome: a reservoir of biomarkers. *J Transl Med* **6**, 52 (2008).

49. Porporato, P. E. Understanding cachexia as a cancer metabolism syndrome. *Oncogenesis* **5**, e200–e200 (2016).

50. Mohammad, S. *et al.* Circulating small extracellular vesicles increase after an acute bout of moderate-intensity exercise in pregnant compared to non-pregnant women. *Sci Rep* **11**, 12615 (2021).

51. Jiang, P., Ren, L., Zhi, L., Hu, X. & Xiao, R.-P. Protocol for cell preparation and gene delivery in HEK293T and C2C12 cells. *STAR Protoc* **2**, 100497 (2021).

52. Ishibashi, A. *et al.* A simple method using CRISPR-Cas9 to knock-out genes in murine cancerous cell lines. *Sci Rep* **10**, 22345 (2020).

53. Wiper-Bergeron, N., Salem, H. A., Tomlinson, J. J., Wu, D. & Haché, R. J. G. Glucocorticoid-stimulated preadipocyte differentiation is mediated through acetylation of C/EBPβ by GCN5. *Proceedings of the National Academy of Sciences* **104**, 2703–2708 (2007).

54. Go, C. D. *et al.* A proximity-dependent biotinylation map of a human cell. *Nature* **595**, 120–124 (2021).

55. Lamarche, É. *et al.* SMAD2 promotes myogenin expression and terminal myogenic differentiation. *Development* **148**, (2021).

56. Hartjes, T., Mytnyk, S., Jenster, G., van Steijn, V. & van Royen, M. Extracellular Vesicle Quantification and Characterization: Common Methods and Emerging Approaches. *Bioengineering* **6**, 7 (2019).

57. Habel, J. E. Biotin Proximity Labeling for Protein–Protein Interaction Discovery: The BioID Method. in 357–379 (2021). doi:10.1007/978-1-0716-1186-9_22.

58. Guo, J. *et al.* The development of proximity labeling technology and its applications in mammals, plants, and microorganisms. *Cell Communication and Signaling* **21**, 269 (2023).

59. Li, Y., Kanao, E., Yamano, T., Ishihama, Y. & Imami, K. TurboID-EV: Proteomic Mapping of Recipient Cellular Proteins Proximal to Small Extracellular Vesicles. *Anal Chem* **95**, 14159–14164 (2023).

60. Sears, R. M., May, D. G. & Roux, K. J. BioID as a Tool for Protein-Proximity Labeling in Living Cells. in 299–313 (2019). doi:10.1007/978-1-4939-9546-2_15.

61. Schiapparelli, L. M. *et al.* Direct Detection of Biotinylated Proteins by Mass Spectrometry. *J Proteome Res* **13**, 3966–3978 (2014).

62. Kim, J., Cantor, A. B., Orkin, S. H. & Wang, J. Use of in vivo biotinylation to study protein–protein and protein–DNA interactions in mouse embryonic stem cells. *Nat Protoc* **4**, 506–517 (2009).

63. de Boer, E. *et al.* Efficient biotinylation and single-step purification of tagged transcription factors in mammalian cells and transgenic mice. *Proceedings of the National Academy of Sciences* **100**, 7480–7485 (2003).

64. Guo, J. *et al.* The development of proximity labeling technology and its applications in mammals, plants, and microorganisms. *Cell Communication and Signaling* **21**, 269 (2023).

65. Chitti, S. V. *et al.* Proteomic analysis of the small extracellular vesicles and soluble secretory proteins from cachexia inducing and non-inducing cancer cells. *Proteomics* **23**, (2023).

66. Rubartelli, A., Bajetto, A., Allavena, G., Wollman, E. & Sitia, R. Secretion of thioredoxin by normal and neoplastic cells through a leaderless secretory pathway. *J Biol Chem* **267**, 24161–4 (1992).

67. Powis, G. & Kirkpatrick, D. L. Thioredoxin signaling as a target for cancer therapy. *Curr Opin Pharmacol* **7**, 392–397 (2007).

68. Silva, A. *et al.* Prognostic Value of Monocarboxylate Transporter 1 Overexpression in Cancer: A Systematic Review. *Int J Mol Sci* **24**, 5141 (2023).

69. Madan, B., Virshup, D. M., Nes, W. D. & Leaver, D. J. Unearthing the Janus-face cholesterogenesis pathways in cancer. *Biochem Pharmacol* **196**, 114611 (2022).

70. Fang, R., Yan, L. & Liao, Z. Abnormal lipid metabolism in cancer-associated cachexia and potential therapy strategy. *Front Oncol* **13**, 1123567 (2023).

71. Melloni, E., Salamino, F. & Sparatore, B. The calpain-calpastatin system in mammalian cells: properties and possible functions. *Biochimie* **74**, 217–223 (1992).

72. Wu, J. *et al.* Synergic effect of PD-1 blockade and endostar on the PI3K/AKT/mTOR-mediated autophagy and angiogenesis in Lewis lung carcinoma mouse model. *Biomedicine & Pharmacotherapy* **125**, 109746 (2020).

73. He, Q., Sun, C. & Pan, Y. Whole-exome sequencing reveals Lewis lung carcinoma is a hypermutated Kras/Nras–mutant cancer with extensive regional mutation clusters in its genome. *Sci Rep* **14**, 100 (2024).

74. Shields, N. J. *et al.* Late-stage MC38 tumours recapitulate features of human colorectal cancer - implications for appropriate timepoint selection in preclinical studies. *Front Immunol* **14**, 1152035 (2023).

75. Efremova, M. *et al.* Targeting immune checkpoints potentiates immunoediting and changes the dynamics of tumor evolution. *Nat Commun* **9**, 32 (2018).

76. Lechner, M. G. *et al.* Immunogenicity of Murine Solid Tumor Models as a Defining Feature of In Vivo Behavior and Response to Immunotherapy. *Journal of Immunotherapy* **36**, 477–489 (2013).

77. Zhong, W. *et al.* Comparison of the molecular and cellular phenotypes of common mouse syngeneic models with human tumors. *BMC Genomics* **21**, 2 (2020).

78. Kienzl, M. *et al.* Comparative Study of the Immune Microenvironment in Heterotopic Tumor Models. *Cancers (Basel)* **16**, (2024).

79. Zhang, G. *et al.* Tumor induces muscle wasting in mice through releasing extracellular Hsp70 and Hsp90. *Nat Commun* **8**, 589 (2017).

80. Bae, T. *et al.* Paeonia lactiflora root extract suppresses cancer cachexia by down-regulating muscular NF-κB signalling and muscle-specific E3 ubiquitin ligases in cancer-bearing mice. *J Ethnopharmacol* **246**, 112222 (2020).

81. Schäfer, M. *et al.* Ataxin-10 is part of a cachexokine cocktail triggering cardiac metabolic dysfunction in cancer cachexia. *Mol Metab* **5**, 67–78 (2016).

82. Huot, J. R., Pin, F., Essex, A. L. & Bonetto, A. MC38 Tumors Induce Musculoskeletal Defects in Colorectal Cancer. *Int J Mol Sci* **22**, 1486 (2021).

83. Pryce, B. R., Wang, D. J., Zimmers, T. A., Ostrowski, M. C. & Guttridge, D. C. Cancer cachexia: involvement of an expanding macroenvironment. *Cancer Cell* **41**, 581–584 (2023).

84. Zhang, G., Jin, B. & Li, Y.-P. C/EBPβ mediates tumour-induced ubiquitin ligase atrogin1/MAFbx upregulation and muscle wasting. *EMBO J* **30**, 4323–4335 (2011).

85. Chen, M.-H. *et al.* Gut microbiota influenced the xenograft MC38 tumor growth potentially through interfering host lipid and amino acid metabolisms, basing on the integrated analysis of microbiome and metabolomics. *Journal of Chromatography B* **1192**, 123136 (2022).

86. Voltarelli, F. A. *et al.* Syngeneic B16F10 Melanoma Causes Cachexia and Impaired Skeletal Muscle Strength and Locomotor Activity in Mice. *Front Physiol* **8**, 715 (2017).

87. Huot, J. R. *et al.* GL261 glioblastoma induces delayed body weight gain and stunted skeletal muscle growth in young mice. *American Journal of Physiology-Regulatory, Integrative and Comparative Physiology* **328**, R628–R641 (2025).

88. Rodriguez, G. M. *et al.* The Tumor Immune Profile of Murine Ovarian Cancer Models: An Essential Tool for Ovarian Cancer Immunotherapy Research. *Cancer Research Communications* **2**, 417–433 (2022).

89. RAMJI, D. P. & FOKA, P. CCAAT/enhancer-binding proteins: structure, function and regulation. *Biochemical Journal* **365**, 561–575 (2002).

90. Tang, Q.-Q. *et al.* Sequential phosphorylation of CCAAT enhancer-binding protein β by MAPK and glycogen synthase kinase 3β is required for adipogenesis. *Proceedings of the National Academy of Sciences* **102**, 9766–9771 (2005).

91. Phillips, T. Regulation of Transcription and Gene Expression in Eukaryotes. *Nature Education* **1**, 199 (2008).

92. Moses, J., Goodchild, A. & Rivory, L. P. Intended transcriptional silencing with siRNA results in gene repression through sequence-specific off-targeting. *RNA* **16**, 430–41 (2010).

93. Li, Y. & Zhou, L. dCas9 techniques for transcriptional repression in mammalian cells: Progress, applications and challenges. *BioEssays* **43**, (2021).

94. Williams, S. C., Angerer, N. D. & Johnson, P. F. C/EBP proteins contain nuclear localization signals imbedded in their basic regions. *Gene Expr* **6**, 371–85 (1997).

95. Falkenberg, K. D. *et al.* Withaferin A, a natural compound with anti-tumor activity, is a potent inhibitor of transcription factor C/EBPβ. *Biochimica et Biophysica Acta (BBA) - Molecular Cell Research* **1864**, 1349–1358 (2017).

96. Darvishi, E. *et al.* Anticancer Activity of ST101, A Novel Antagonist of CCAAT/Enhancer Binding Protein β. *Mol Cancer Ther* **21**, 1632–1644 (2022).

97. Abdel Ghani, L. *et al.* A synthetic covalent ligand of the C/EBPβ transactivation domain inhibits acute myeloid leukemia cells. *Cancer Lett* **530**, 170–180 (2022).

98. Sherman, C. D., Lodha, S. & Sahoo, S. EV Cargo Sorting in Therapeutic Development for Cardiovascular Disease. *Cells* **10**, (2021).

99. van de Wakker, S. I. *et al.* Size matters: Functional differences of small extracellular vesicle subpopulations in cardiac repair responses. *J Extracell Vesicles* **13**, (2024).

100. Kalluri, R. & McAndrews, K. M. The role of extracellular vesicles in cancer. *Cell* **186**, 1610–1626 (2023).

101. Wang, Y. & Ding, S. Extracellular vesicles in cancer cachexia: deciphering pathogenic roles and exploring therapeutic horizons. *J Transl Med* **22**, 506 (2024).

102. Battistelli, M. & Falcieri, E. Apoptotic Bodies: Particular Extracellular Vesicles Involved in Intercellular Communication. *Biology (Basel)* **9**, (2020).

103. Penet, M.-F. & Bhujwalla, Z. M. Cancer cachexia, recent advances, and future directions. *Cancer J* **21**, 117–22 (2015).

104. Kubitz, L. *et al.* Engineering of ultraID, a compact and hyperactive enzyme for proximity-dependent biotinylation in living cells. *Commun Biol* **5**, 657 (2022).

105. Ham, B. M. *et al.* The influence of sample preparation and replicate analyses on HeLa Cell phosphoproteome coverage. *J Proteome Res* **7**, 2215–21 (2008).

106. Karlenius, T. C. & Tonissen, K. F. Thioredoxin and Cancer: A Role for Thioredoxin in all States of Tumor Oxygenation. *Cancers (Basel)* **2**, 209–32 (2010).

107. Muri, J., Thut, H., Feng, Q. & Kopf, M. Thioredoxin-1 distinctly promotes NF-κB target DNA binding and NLRP3 inflammasome activation independently of Txnip. *Elife* **9**, (2020).

108. Cornwell, E. W., Jackman, R. W., Mirbod, A. & Kandarian, S. C. The role of NF-kappaB in cancer cachexia-induced skeletal muscle wasting. *The FASEB Journal* **25**, (2011).

109. Liu, C. *et al.* Prognostic significance and biological function of Lamina-associated polypeptide 2 in non-small-cell lung cancer. *Onco Targets Ther* **12**, 3817–3827 (2019).

110. Bennati, A. M. *et al.* Disruption of the gene encoding 3beta-hydroxysterol Delta-reductase (Tm7sf2) in mice does not impair cholesterol biosynthesis. *FEBS J* **275**, 5034–47 (2008).

111. Tsai, P.-L., Zhao, C., Turner, E. & Schlieker, C. The Lamin B receptor is essential for cholesterol synthesis and perturbed by disease-causing mutations. *Elife* **5**, (2016).

112. Xia, W. *et al.* The role of cholesterol metabolism in tumor therapy, from bench to bed. *Front Pharmacol* **14**, (2023).

113. Roy, A. & Kumar, A. ER Stress and Unfolded Protein Response in Cancer Cachexia. *Cancers (Basel)* **11**, (2019).

114. Blomme, A. *et al.* Myoferlin is a novel exosomal protein and functional regulator of cancer-derived exosomes. *Oncotarget* **7**, 83669–83683 (2016).

115. Chiu, M., Taurino, G., Bianchi, M. G., Kilberg, M. S. & Bussolati, O. Asparagine Synthetase in Cancer: Beyond Acute Lymphoblastic Leukemia. *Front Oncol* **9**, (2020).

116. Jin, H. *et al.* Asparagine synthetase regulates the proliferation and differentiation of chicken skeletal muscle satellite cells. *Anim Biosci* **37**, 1848–1862 (2024).

117. Inaba, S., Hinohara, A., Tachibana, M., Tsujikawa, K. & Fukada, S.-I. Muscle regeneration is disrupted by cancer cachexia without loss of muscle stem cell potential. *PLoS One* **13**, e0205467 (2018).

118. Pin, F. *et al.* Interference with Ca2+-Dependent Proteolysis Does Not Alter the Course of Muscle Wasting in Experimental Cancer Cachexia. *Front Physiol* **8**, 213 (2017).

119. Pandurangan, M. & Hwang, I. The role of calpain in skeletal muscle. *Anim Cells Syst (Seoul)* **16**, 431–437 (2012).

120. Liu, J., Jang, J. Y., Pirooznia, M., Liu, S. & Finkel, T. The secretome mouse provides a genetic platform to delineate tissue-specific in vivo secretion. *Proceedings of the National Academy of Sciences* **118**, (2021).

121. Brown, K. J. *et al.* Advances in the proteomic investigation of the cell secretome. *Expert Rev Proteomics* **9**, 337–345 (2012).

122. Tammela, T. & Sage, J. Investigating Tumor Heterogeneity in Mouse Models. *Annu Rev Cancer Biol* **4**, 99–119 (2020).

123. Pinto, C., Estrada, M. F. & Brito, C. In Vitro and Ex Vivo Models – The Tumor Microenvironment in a Flask. in 431–443 (2020). doi:10.1007/978-3-030-34025-4_23.

124. Wei, W. *et al.* Cell type-selective secretome profiling in vivo. *Nat Chem Biol* **17**, 326–334 (2021).

125. Oliver, A. J. *et al.* Tissue-Dependent Tumor Microenvironments and Their Impact on Immunotherapy Responses. *Front Immunol* **9**, (2018).

126. Deshmukh, A. S. *et al.* Deep Proteomics of Mouse Skeletal Muscle Enables Quantitation of Protein Isoforms, Metabolic Pathways, and Transcription Factors*. *Molecular & Cellular Proteomics* **14**, 841–853 (2015).

127. Yang, W. *et al.* Molecular mechanisms of cancer cachexia-induced muscle atrophy (Review). *Mol Med Rep* **22**, 4967–4980 (2020).

128. WATANABE, H. & OSHIMA, T. The Latest Treatments for Cancer Cachexia: An Overview. *Anticancer Res* **43**, 511–521 (2023).